

AN ABSTRACT OF A THESIS

SURFACE TOPOLOGY-INDUCED ULTRAHYDROPHOBIC BEHAVIOR: EFFECT OF THREE-PHASE CONTACT LINE TOPOLOGY

Neeharika Anantharaju

Master of Science in Mechanical Engineering

The wettability characteristics of silicon surfaces hydrophobized using silanization reagents were studied. The advancing and receding contact angles were measured with the captive needle approach and were compared with the previously published results. Further, the wetting behavior of water droplets on periodically-structured hydrophobic surfaces was investigated. The surfaces were prepared by the wet etching process and contain poles and holes of different sizes and area void fractions. The surface geometry made possible studying both Wenzel (filling of surface grooves) and Cassie (non-filling of surface grooves) states and the effects of surface geometry and roughness on the contact angle in these states. Experimental data point to an anomalous behavior where the data do not obey either Wenzel or Cassie type phenomenology for surfaces with holes. This behavior is explained by an understanding of the three-phase contact line topology which is continuous for the specimen with holes and discontinuous for the specimen with poles. The effect of contact line topology on the contact angle was thus parametrically studied. The observations may serve as guidelines in designing surfaces with the desired wetting behavior.

**SURFACE TOPOLOGY-INDUCED ULTRAHYDROPHOBIC
BEHAVIOR: EFFECT OF THREE-PHASE CONTACT LINE
TOPOLOGY**

A Thesis

Presented to

The Faculty of the Graduate School

Tennessee Technological University

by

Neeharika Anantharaju

In Partial Fulfillment

Of the Requirements for the Degree

MASTER OF SCIENCE

Mechanical Engineering

August 2007

CERTIFICATE OF APPROVAL OF THESIS

**SURFACE TOPOLOGY-INDUCED ULTRAHYDROPHOBIC
BEHAVIOR: EFFECT OF THREE-PHASE CONTACT LINE
TOPOLOGY**

By

Neeharika Anantharaju

Graduate Advisory Committee:

Mahesh V. Panchagnula, Chairperson

Date

Sastry Munukutla

Date

John Peddieson, Jr.

Date

Approved for the Faculty:

Francis Otuonye
Associate Vice President for
Research and Graduate Studies

Date

STATEMENT OF PERMISSION TO USE

In presenting this thesis in partial fulfillment of the requirements for a Master of Science Degree at Tennessee Technological University, I agree that the University Library shall make it available to borrowers under rules of the Library. Brief quotations from this thesis are allowable without special permission, provided that accurate acknowledgement of the source is made.

Permission for extensive quotation from or reproduction of this thesis may be granted by my major professor when the proposed use of the material is for scholarly purposes. Any copying of the material in this thesis for financial gain shall not be allowed without my written permission.

Signature _____

Date _____

ACKNOWLEDGEMENTS

I take this opportunity to thank the people who have been an integral part of my graduate education.

It has been a pleasure to work with an advisory committee that has been a great source of inspiration. I am very thankful to my research advisor Dr. Mahesh V. Panchagnula for his invaluable guidance and teaching, tremendous patience, and motivation, throughout the research. I am indebted to Dr. Sastry Munukutla for being extremely supportive throughout my graduate study. I would like to thank Dr. John Peddieson for being a member of my graduate advisory committee.

I deeply appreciate Mr. Wayne Kimsey for his valuable and continuous assistance with the data analysis. I also thank Mr. David Walker who helped me in setting up the experimental apparatus.

I acknowledge the support of Center for Energy Systems Research (CESR) and the Department of Mechanical Engineering through my graduate study.

I would like to thank all my friends and well wishers for just being there.

Lastly, and most importantly, I would like to express my heartfelt gratitude to my parents, Leelamohan Rao and Madhavi, and my sister and friend Himabindu, for their constant support, encouragement, patience, and love. To them I dedicate this thesis.

TABLE OF CONTENTS

	Page
LIST OF FIGURES	vi
CHAPTER 1 - Introduction	1
CHAPTER 2 - Literature Review	8
2.1 Structured Surfaces	11
2.2 Unstructured Surfaces	14
2.3 Theoretical Studies	18
2.4 Thesis Objective.....	20
CHAPTER 3 - Experimental Approach	21
3.1 Chemicals and Materials	21
3.2 Contact Angle Measurement	23
CHAPTER 4 - Results and Discussion.....	28
4.1 Heterogeneous Wetted State Results.....	30
4.1.1 Summary	34
4.2 Homogenous Wetted State Results	35
4.2.1 Summary	37
4.3 Discussion.....	38
CHAPTER 5 - Conclusions and Recommendations	57
5.1 <i>Conclusions</i>	57
5.2 Recommendations	59

LIST OF FIGURES

	Page
Figure 1.1 Sessile drop of liquid on a surface exhibiting the three interfacial energies and the contact angle.....	7
Figure 1.2 Hydrophobic, hydrophilic, and superhydrophobic water drops.....	7
Figure 1.3 Homogeneous (Wenzel) and heterogeneous (Cassie) wetting of water drops on a surface with poles.....	7
Figure 3.1 SEM images of the specimen with ‘holes’ and ‘poles’.....	26
Figure 3.2 Hydrolytic depositions of silanes (courtesy: Gelest, Inc., manual).....	26
Figure 3.3 Image of a hydrophobic drop with the captive needle.....	27
Figure 3.4 Contact Angle Goniometer.....	27
Figure 3.5 MATLAB program output.....	28
Figure 4.1 Contact angle versus area void fraction for varying characteristic length, ‘a’ (H=30 microns).....	44
Figure 4.2 Contact angle versus area void fraction for varying ‘a’ (H=3 microns).....	45
Figure 4.3 Contact angle versus ‘a’ for varying area void fraction (H=30microns).....	46
Figure 4.4 Contact angle versus ‘a’ for varying area void fraction (H- 3microns).....	47
Figure 4.5 Contact angle hysteresis versus Area void fraction for characteristic length, ‘a’ = 20 microns (H=30 microns).....	48
Figure 4.6 Contact angle hysteresis versus ‘a’ for area void fraction, f=0.75 (H=30 microns).....	49
Figure 4.7 Contact angle versus roughness, r (H=30 microns).....	50

Figure 4.8 Contact angle versus roughness, r ($H=3$ microns).....	51
	Page
Figure 4.9 Measured contact angles versus calculated contact angles ($H=30$ microns). ..	52
Figure 4.10 Measured contact angles versus calculated contact angles ($H=3$ microns) ...	53
Figure 4.11 Contact line on surface with square and circular holes. The images above depict contact circle before the pinning and the images below depict pinned contact line.....	54
Figure 4.12 Pinning force per unit length of the contact line f_p' versus area void fraction, f for surfaces with circular and square cavities.....	55
Figure 4.13 Comparison of data from Abdelsalam et al. against Cassie-Baxter theory and current theory.....	56

CHAPTER 1

INTRODUCTION

Wettability of solid surfaces is an important physical phenomenon in fluid mechanics and heat transfer. It is usually characterized by the contact angle exhibited by a liquid drop placed on the solid surface termed as the sessile drop condition. The contact angle that a sessile drop makes on a solid surface may be experimentally observed to take on a wide range of values owing to the nature of the process of placing the sessile drop. There exist maximum and minimum stable contact angles that this drop can manifest and all the intermediate angles are metastable states. These maximum and minimum values are referred to as the advancing and receding angles of the drop. On increasing (decreasing) the volume of the drop, the wetted radius of the drop will increase (decrease) to manifest an asymptotic advancing (receding) stable contact angle. The difference between the advancing and the receding angles is termed Contact Angle Hysteresis (CAH) and can broadly be defined as the “tilt” angle that the solid specimen with a sessile drop can bear before the drop begins to roll off. This is an important property, as a lower CAH accounts for higher drop mobility. Such surfaces find many applications including self cleaning ability.

The basis of CAH is usually attributed to the failure of the system to meet the conditions of ideality like smoothness, rigidity, chemical and physical homogeneity of solid, etc. Thus, the most commonly attributed causes of CAH are roughness, topology, microporosity of solids, microscopic heterogeneity of the solid, reorientation of the

molecules and groups, and transfer of molecules from liquid across the solid surface either by surface diffusion or evaporation.

On an ideal smooth chemically homogenous surface, i.e. a surface with no hysteresis, the contact angle that a sessile drop of liquid exhibits is believed to be governed by the minimum of the total Gibbs free energy (liquid/solid + liquid/vapor + solid/vapor interfacial free energies). Consider a sessile drop on a homogenous surface (see Figure 1.1). The interfacial free energies per unit area of the solid-liquid, liquid-vapor, and solid-vapor interfaces are represented by γ_{SL} , γ_{LV} , and γ_{SV} . Let the solid-liquid interfacial area be increased by dA by wetting. On wetting the surface, the interfacial energy contributions are changed by $\gamma_{SL} dA$, $\gamma_{LV} (\cos\theta)dA$, and $-\gamma_{SV} dA$, respectively. The liquid-vapor interfacial energy is related to the contact angle that the liquid drop makes on the surface owing to the geometry of the drop being a part of a sphere. Thus the change in the Gibbs free energy of the system is given by

$$dE = \gamma_{SL} dA - \gamma_{SV} dA + \gamma_{LV} \cos\theta dA \quad 1.1$$

The sessile drop comes to rest or reaches a stable contact angle when the minimum of the total Gibbs free energy is reached i.e

$$\frac{dE}{dA} = 0 \quad 1.2$$

Thus, for the equilibrium state, Equation (1) can be written as

$$\gamma_{SL} - \gamma_{SV} + \gamma_{LV} \cos\theta_Y = 0 \quad 1.3$$

where θ_Y is called the Young's thermodynamic contact angle and

Equation 1.3 is the *classical Young's equation* and can be rewritten as

$$\cos \theta_Y = \frac{\gamma_{SV} - \gamma_{SL}}{\gamma_{LV}} \quad 1.4$$

For a drop contact angle, θ greater than the Young's contact angle ($\theta > \theta_Y$), the non-wetted region is unstable. So the energy contribution due to the solid-liquid contact area increases with a corresponding decrease in the solid-vapor interfacial energy by increasing the wetted radius of the liquid drop. This results in a decrease in the contact angle to reach the stable Young's contact angle for a constant drop volume. Similarly, for a contact angle smaller than the Young's contact angle ($\theta < \theta_Y$), the wetted region is unstable. The energy contribution due to the solid-liquid contact area decreases with a corresponding increase in the solid-vapor interfacial energy by decreasing the wetted radius of the liquid drop. This results in an increase in the contact angle to attain the Young's stable contact angle.

The contact angle itself is an indicator of the nature of the solid-liquid interaction. In this context, a surface is referred to as being *hydrophobic* when it is less likely to be wetted by water and *hydrophilic* when the surface prefers being wetted by water. A hydrophilic surface exhibits a contact angle less than 90° while a hydrophobic surface exhibits an angle greater than 90° . A hydrophobic surface exhibiting a stable contact angle greater than 150° is said to be *superhydrophobic* (see Figure 1.2). Superhydrophobic surfaces are therefore surfaces with low CAH and high θ_Y .

Hydrophobic surfaces can be fabricated using surface treatments which alter the interfacial surface energies, γ_{SV} and γ_{SL} , such as perfluorinated coatings which produce a Young's contact angle in excess of 110° . However, no materials or coatings exist that can generate a Young's contact angle greater than 150° (superhydrophobic surfaces); surface

topology needs to be modified to achieve this effect. The present thesis is restricted to hydrophobic behavior enhancement by surface topology and is based on exploiting the rich physics involved in the dual stable states of wettability- *homogenous* and *heterogeneous* states (see Figure 1.3) of hydrophobic sessile drop behavior. In this context, homogenous wetting is defined as a regime where the liquid completely wets the solid surface, whereas heterogeneous wetting is defined as the case when air (or liquid vapor) is trapped between the sessile liquid drop and the surface. The heterogeneous wetting regime is characterized by lower contact angle hysteresis than homogenous wetting regime, which results in higher drop mobility. The homogenous and heterogeneous wetting regimes are described by the Cassie-Baxter [1] and Wenzel [2] theories, respectively, that are described later in detail.

Roughness enhanced superhydrophobicity (SHP) can be used to achieve remarkably different drop contact angle behavior as compared to unmodified hydrophobic surfaces. A bio-inspired example of such behavior is the lotus leaf. The extreme water repellency demonstrated by the lotus leaf has motivated a large body of biomimetic effort to increase the hydrophobicity of surfaces [3]. Mimicking the surface topology of the lotus leaf, most studies have focused on the effect of microscale polyhedral poles on the contact angle of water drops on the surface (fakir condition) [4].

For example, researchers have created surfaces with uniform arrays of poles fabricated by photolithography techniques [5, 6] or other etching methods [7]. A variety of surface topologies have been studied: square pillars [8], parallel grooves [9-11], and circular pillars [5, 12]. Recent studies [13] as well as SEM images of hydrophobic leaf

surface microstructure have demonstrated the importance of having multiple characteristic length scales to achieve lower contact angle hysteresis.

When the surface is covered by microscale poles between which air is trapped, the surface area in contact with the drop are the top surfaces of the poles. Substituting this in the above free energy equation (1.1) and minimizing, the Cassie-Baxter equation for the apparent contact angle is obtained. The apparent contact angle can be shown to be the weighted average of the contact angle with air (180°) and the Young's contact angle of the plain surface, θ_Y ,

$$\cos(\theta) = (1 - f) \cos(\theta_Y) + f \cos(180^\circ) \quad 1.5$$

where f is the area fraction of the tops of the poles to the total projected area of the surface. The above equation for the contact angle dependence with the area void fraction has been extensively tested by experimental measurements on fakir droplets on surfaces with poles of different cross section shapes and a wide range of length scales. However, this theoretical development does not take into account the topology of the three-phase contact line. In this context, the three-phase contact line is defined as the set of points in contact with the solid, liquid and, vapor phases. The three-phase contact line has been recognized to play an important role in determining the contact angle due to pinning [14] and thus CAH. The Cassie theory in Equation (1.5) is derived purely from Gibbs free energy minimization arguments and hence does not include contact line effects. It is curious that a model which does not account for the three-phase contact line topology has proven so successful in predicting the contact angle dependence on the area void fraction. In addition, most contact angle measurements are performed under dynamic conditions (either advancing or receding). It is even more curious that an equation derived for the

case of a defect-free surface under thermodynamic equilibrium conditions has found success applied to dynamic contact angles [15]. A closer observation shows that in the case of a fakir drop (where Cassie-Baxter theory has found much of its success) the three-phase contact line actually consists of multiple loops around the top of each pole in contact with the drop. Thus the “apparent” three-phase contact line at the advancing edge of the drop (wetted circle circumference) in the case of the drop on a bed of poles is discontinuous. Presumably a continuous advancing three-phase contact line will demonstrate a behavior different from the predictions of the Cassie-Baxter theory due to the possibility of contact line pinning. We test this possibility experimentally by measuring the contact angle on surfaces with holes as well as poles. It is easily seen that in the case of surfaces with holes, the three-phase contact line will lie on the surface between the holes and hence will be continuous.

An outline of the remainder of the thesis is as follows. Chapter 2 summarizes the wide body of research developed towards fundamental and ground-breaking applications due to surface tension properties, highlighting the aspects relevant to the current study. Chapter 3 discusses the experimental technique involved in fabricating the microstructured surfaces varying in area void fraction and characteristic length scales and the procedure involved in measuring the contact angles on the surfaces used in the current study. Chapter 4 discusses in detail the results obtained through this course of experimentation. Chapter 5 provides the conclusions from the present work and recommendations for future studies.

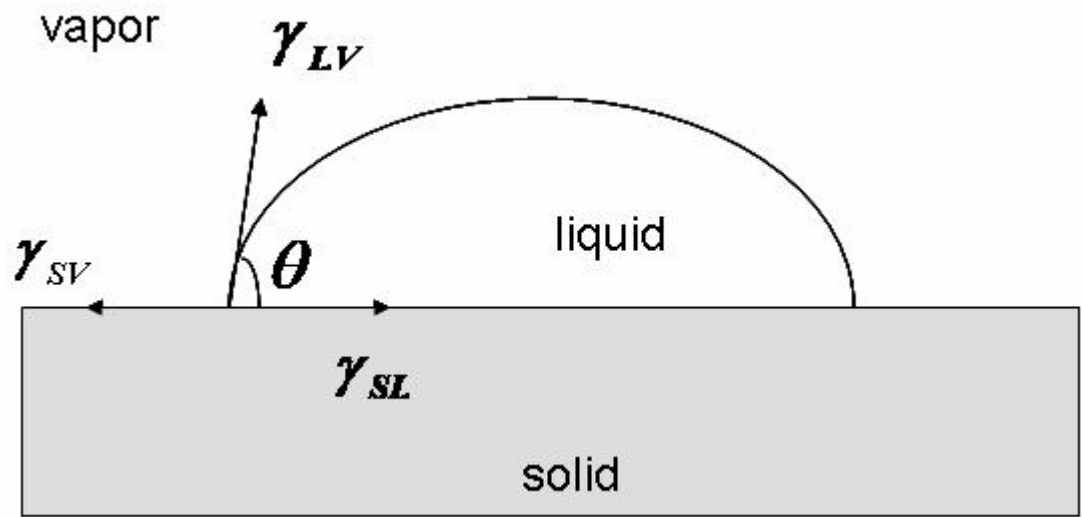


Figure 1.1 Sessile drop of liquid on a surface exhibiting the three interfacial energies and the contact angle.



Figure 1.2 Hydrophobic, hydrophilic, and superhydrophobic water drops.



Figure 1.3 Homogeneous (Wenzel) and heterogeneous (Cassie) wetting of water drops on a surface with poles.

CHAPTER 2

LITERATURE REVIEW

‘Hydrophobic’ and ‘Hydrophilic’ are the frequently used descriptors for surfaces to characterize their interaction with water. A surface is referred to as being hydrophobic when it is less likely to be wetted by water and hydrophilic when the surface prefers being wetted by water. The wettability behavior can be quantitatively analyzed based on the sessile drop contact angle on the surface. A surface is said to be *Hydrophilic* when the contact angle is less than 90° , *Hydrophobic* for an angle greater than 90° , and *Superhydrophobic (SHP)* for angles greater than 150° . The properties of SHP surfaces such as water-repellency and self-cleaning give rise to a wide range of novel applications. Motivated by behavior of the lotus leaf from nature, a vast body of research has recently been developed towards radical and innovative applications due to surface tension properties and phase change characteristics. This chapter summarizes such research, highlighting the aspects relevant to the current study.

The earliest direct observation of wetting phenomenon was made by Galileo. Almost 200 years after Galileo, Thomas Young [16] developed the concept of surface tension and contact angle and developed an equation (see Equation (1.3)) relating the contact angle to surface energy contributions from the solid-vapor interface (γ_{sv}), solid-liquid interface (γ_{sl}), and liquid-vapor interface (γ_{lv}).

Many methods have been developed to measure contact angles. A discussion of ‘Contact Angle Hysteresis’ (CAH) and the need for it is first of interest. The concept of contact angle hysteresis (CAH) was established almost 70 years ago [17] and is defined

as the difference between the ‘advancing’ or ‘recently advanced’ contact angle, θ_a and the ‘receding’ or ‘recently receded’ contact angle, θ_r i.e.

$$\text{CAH} = \theta_a - \theta_r \quad 2.2$$

In real system, H is a measure of the mobility of a drop on the surface. The causes of CAH are manifold including roughness, topology, microporosity of solids, microscopic chemical heterogeneity of the solid, re-orientation of the molecules and groups, and transfer of molecules from liquid across the solid surface either by surface diffusion or evaporation. The need for taking into account the hysteresis in contact angles was brought light by Oner and McCarthy [4].

Several techniques have been developed to measure the advancing and receding angles. The first of them is due to Zisman [18, 19] in which the tip of a fine platinum wire was used to bring a drop into contact with a surface and successively add and remove drop volume, thus obtaining the limiting values of contact angles. A second technique developed in Good’s laboratory [16] involved the drop being introduced by means of a micrometer syringe with a fine needle, which is held captive while additional liquid was added to or removed from the drop. A third method to measure CAH uses a support plate that can be tilted. When the plate surface reaches a critical slope such that the drop is on the verge of motion, the angle measured at the downhill and uphill edges of the drop may approach the advancing and receding angles, respectively. The difference between the two angles at an inclination, beyond which the drop starts to slide down the slope, is measured as CAH. The drawback with these methods was the dependence of contact angle on drop size, especially while measuring the receding angle [20-22]. A method closer to the captive sessile drop technique was the captive bubble technique that

had a bubble of gas at the tip of the micrometer syringe which was pressed onto the solid. Gas added to the bubble causes the liquid front to retreat and withdrawing the gas causes the liquid front to advance. This method, however, gave a contact angle that tends to be closer to the receding angle. Another method worth mentioning is the Wilhelmy plate method [23]. This technique involves a rectangular sheet of material under test suspended from an electrobalance beam. The beaker of liquid whose contact angle needs to be measured was raised and lowered at a preset rate. The force for withdrawing the plate varied as $\cos \theta$, where θ is the contact angle. This method yielded receding angles just as easily as advancing angles but was not very practical due to the drawback that it had to consider average values over an entire parametric line of intersection of liquid with the solid. If the front and back faces were different in the chemical treatment, the average value may have little significance.

Of all the techniques outlined above, the captive needle approach is the most practical and was made error free by increasing and decreasing the volume of water at a known rate using a precision syringe pump. In the present study, the asymptotic advancing and receding angles were measured using this captive needle approach.

Hydrophobic surfaces can be fabricated using surface treatments which alter wettability, such as perfluorinated coatings with the resulting equilibrium contact angle of 119° . However no surface treatments currently exist that can generate an equilibrium contact angle approaching 150° which is typical of SHP surfaces; surface topology needs to be modified in order to achieve this effect. The present thesis deals with the study of hydrophobic behavior being altered due to surface topology. In the current study,

specimens of varying structured ‘roughness’ were created on a silicon wafer through a wet-etch process. The specimens were hydrophobized by a silanization process [4].

Surface topology effects on hydrophobic behavior has been studied extensively since the original work on homogeneous wetting by Wenzel [2] and heterogeneous wetting by Cassie [1], the dual stable states of existence of the hydrophobic drop behavior. Homogeneous wetting, also referred to as the Wenzel state, is defined as the regime where the liquid completely wets the solid surface whereas heterogeneous wetting, also referred to as the Cassie state, is defined as the case when air (or liquid vapor) is trapped between the sessile liquid drop and the surface. The heterogeneous wetting regime is characterized by lower contact angle hysteresis than the homogeneous wetting regime, which results in higher drop mobility.

Recent work on the effect of surface topology effects on SHP has been focused in three directions- structured, unstructured, and theoretical. These are discussed, in turn, below.

2.1 Structured Surfaces

When the surface roughness is definable by a simple geometric representation, it is referred to as structured surface. Some representative studies are summarized in this sub-section.

Patankar et al. [8] created surfaces with a structured surface topology of square pillars on which they investigated the CAH of sessile drops in the Cassie and Wenzel

states. The drops in the Cassie state were observed to exhibit a much lesser hysteresis and thus proved to be preferred in applications involving high mobility surfaces.

He et al. [11] studied wettability of poly (dimethylsiloxane) (PDMS) surfaces with square pillars of different dimensions fabricated by micromachining techniques [24]. The PDMS surfaces were sputter coated with gold and contact angle measurements were carried out by a goniometer. On the basis of experimental evidence, the existence of two contact angles on the same roughness surface, modeled by the Cassie and Wenzel theories, depending on how a drop is formed, was shown. Also, a design criterion was established according to which, for a robust hydrophobic rough surface, the apparent contact angle will not change due to external disturbance.

Chen et al. [10] reported a theoretical and experimental study of wetting of surfaces with parallel groove geometry. The primary objective of this work was to determine the mechanism of anisotropic wetting and to propose a methodology to quantify the apparent contact angles and the drop shape.

Iwamatsu [25] studied the behavior of drops on heterogeneous striped surfaces. Initially, the contact angle of a drop on a heterogeneous surface is studied under constant volume conditions. By assuming a cylindrical liquid-vapor surface and minimizing the total free energy, an equation for the contact angle was derived which was similar but different from the Cassie's law. On applying this modified Cassie's law to the homogeneous striped surface, it was found that with an increase in the drop volume (advancing contact lines), the predominant drop configuration was observed to have a large contact angle and for a decrease in the drop volume (receding contact lines), the drop configuration was observed to have a lower contact angle. Similar work was

reported by Zhai et al. [5], who created superhydrophobic surfaces fabricated by photolithography techniques with the structured roughness in the form of circular pillars.

The contact angle appears to be related to characteristic roughness length scale and surface void fraction. Oner and McCarthy [4] have studied the effects of topographic length scales on wettability. They stressed the importance of the topology of the three-phase contact line and discussed hydrophobicity from the perspective of the force required to move a water droplet on a surface. Rough silicon surfaces were prepared by photolithography and by hydrophobizing using silanization reagents. These surfaces were posts that varied in sizes, shapes, and separations. Contact angles were measured as a function of the characteristic length and void fraction. An increase in the receding angles was observed by increasing the distance between poles and changing the shape of the poles from square to staggered rhombus, star or indented square. The contact angles were also observed to increase with increase in the tortuosity of the contact line.

Most of the literature involving structured roughness has included only a single length scale to describe the roughness. However, it has been shown recently that SHP behavior in natural systems is attributed to multiple characteristic length scales. Gao and McCarthy [13] recently created rhombus poles which were hydrophobized using two methods- firstly, by using a dimethyldichlorosilane reaction in the vapor phase that introduces a smooth modified layer and secondly, by a solution reaction using methyltrichlorosilane that imparts a second length scale of topology. It was observed that the smooth modified surface exhibited advancing and receding angles of 176° and 156° , respectively, and that the hysteresis was due to the pinning of the receding contact line by the poles. The second length scale was observed to have increased the advancing and

receding angles to angles greater than 176° with little hysteresis. This increase in the advancing angle was also observed to increase the Laplace pressure above which the water intrudes between the poles causing increased hysteresis. This phenomenon is a second reason highlighting the importance of having multiple scales of topology. Similar work was also reported by Cheng et al. [26] who studied the effect of micro- and nano-structures on the self-cleaning behavior of lotus leaves by altering the surface structure of the leaves while keeping their chemical composition approximately unchanged. This study contributed to understanding the behavior of the micro and nanoscale topology and the phenomenon of wetting.

2.2 Unstructured Surfaces

Several studies have reported on various methods that can be used to modify the surface topology to manifest SHP behavior. These range from chemical alteration to growth or deposition of nanoscale structures resulting in stable heterogeneous wetting.

Baldacchini et al. [7] created surfaces with uniform arrays of poles fabricated by etching. They presented a simple method for fabricating superhydrophobic silicon surfaces which consisted of irradiating silicon wafers with femtosecond laser pulses. The surfaces were then coated with a layer of fluoroalkylsilane molecules. The laser irradiation created a surface morphology that exhibited structure on the micro- and nanoscales. By varying the laser fluence, the surface morphology and the wetting properties were tuned. The static and dynamic wetting properties of these surfaces for both water and hexadecane were measured and it was found that both liquids exhibited

contact angles that obeyed the Cassie-Baxter model. The morphology was also observed to be controlled easily allowing for the design of silicon surfaces with different wetting properties. Also, water was observed to exhibit contact angles greater than 160° and with negligible hysteresis. The micro structuring led to transition from nonwetting to wetting in case of hexadecane.

Lacroix et al. [27] reported on a modification of a rough surface with a fluorocarbon coating to render the surface hydrophobic. The roughness was induced by over-etching of a photoresist layer by a SF plasma treatment. The different layers thus obtained exhibited contact angles ranging from 102° - 180° depending on the preparation conditions. On obtaining the scanning electron microscopy images of the surface topology, it was observed that the presence of these dendrites on the surface favored the superhydrophobicity characteristics of the films. Cassie and Wenzel state studies were also performed on these surfaces.

Bhushan and Jung [28] have performed an extensive study on the hydrophobicity characteristics of natural leaf surfaces. They were able to separate out the effects of the micro- and nano scale features of the hydrophobic leaves. They also studied hydrophilic leaves for understanding the role of the wax coating and roughness. Measurements were made to study the adhesion and friction properties of both the hydrophobic and hydrophilic leaves and to fully characterize the leaf surfaces using an optical profiler and an atomic/friction force microscope (AFM/FFM). The leaves with nanobumps were observed to exhibit increased hydrophobic nature and friction properties when compared to microbumps.

Feng et al. [29] fabricated superhydrophobic surfaces of polymer nanofibers and differently patterned aligned carbon nanotube (ACNT) films with pure nanostructures. The contact angle on these ACNT films was observed to exhibit super-‘amphiphobicity’ after coating with fluoroalkylsilane, thus increasing the contact angles to values larger than 160° for both water and oil. They further developed a template based on an extrusion method to synthesize a SHP surface of polyacrylonitrine (PAN) nanofibers. These surfaces had nanostructures similar to ACNTs but at much lower surface densities. This fact contributed to a very large fraction of air in the surface, an essential contributor to Cassie state SHP behavior. This increased the contact angles to values as high as 178° without any modification of the surface by materials of low surface energy. This needle like structure was observed to be ideal for SHP but the hysteresis, a vital parameter contributing to SHP, was also observed to be greater than 30° for surfaces with both the ACNT and PAN nanofibers. The reason for this was hypothesized to involve pinning of the water droplets on these nanostructured surfaces. They further studied the surfaces of rice leaves. These surfaces were observed to exhibit an anisotropic dewetting tendency which might be due to the arrangement of the micropapillae on the surface influencing the motion of the water droplets. This arrangement of the micropapillae was observed to influence the three-phase contact line. They concluded from their work that the nanostructures were essential to achieving high contact angles and that the multiscale structures help in drop mobility and lower hysteresis, the two major factors that characterize SHP behavior.

Hikita et al. [30] developed a one-step sol-gel coating technology which is of practical potential for fabricating super-liquid-repellent surfaces of large areas. Sol-gel

films were prepared by hydrolysis and condensation of alkoxy silane compounds containing colloidal silica nanoparticles and fluoroalkylsilane coupling agents, both of which controlled the surface energy and roughness. These films exhibited high contact angles of 150° and 120° for water and dodecane, respectively.

Sol-gel processing and self-assembly (SA) were employed by Shang et al. [31] in fabricating optically transparent superhydrophobic silica based films. Tuning the microstructures of the sol-gels through careful control of hydrolysis and condensation reactions of various silica precursors helped in achieving desired surface roughnesses. The surface chemistry was modified by introducing a monolayer through surface condensation reaction. Such coatings have applications where anti-reflection, optical transparency, and superhydrophobicity are required.

Jia and McCarthy [32] developed SHP surfaces in which controlled growth of silicon dioxide nanoclusters from tris (trimethylsiloxy) chlorosilane (trisTMSiCl) - modified silicon wafers was carried out by sequential exposure of substrates to tetrachlorosilane (SiCl₄) vapor and atmosphere. Controlling the surface density of trisTMS group by reaction kinetics and the number of SiCl₄/water sequential reactions resulted in surfaces with different topographies and wettabilities. Binary mixed surfaces with one component varying in height from 10-80nm was achieved by chemisorption of tridecafluoro- 1, 1, 2, 2-tetrahydrooctyldimethylchlorosilane (FDCS) on the newly grown silica clusters. Chemical etching effectively removed the organic residues resulting in hydrophilic rough silica surfaces. Further modification with FDCS indicated that the wettability can be controlled by nanoscale roughness.

Liu et al. [33] developed a relatively inexpensive and simple method to fabricate a superhydrophobic ZnO film with hierarchical topological surface structure by a Au-catalyzed direct chemical vapor deposition (CVD) method. This surface structure had a sub-microstructure and a nanostructure on it. The composite surface exhibited SHP behavior by virtue of sufficient air being trapped, resulting in a heterogeneous wetting condition.

Qian and Shen [34] introduced a simple strategy for fabricating SHP surfaces on common polycrystalline substrates of aluminum, copper, and zinc. The simple chemical etching technique involved the use of a dislocation etchant that preferentially dissolves the dislocation sites in the grains. These surfaces on subsequent coating with fluoroalkylsilane exhibited water contact angles above 150° and CAH less than 10° .

Zorba et al. [35] studied the wettability properties of silicon wafers by developing micro-scale and nano-scale structures by femtosecond (fs) laser irradiation. By varying the laser fluence, it was possible to control the surface wettability through systematic and reproducible variation of the surface roughness. The partially trapped air inside resulted in increase of the water-silicon contact angles from 66° to 130° .

2.3 Theoretical Studies

Several studies have applied the free energy balance of the liquid-solid, liquid-vapor, and solid-vapor interfacial energies to characterize the contact angle behavior. These studies have attempted to model surface roughness as being structured with either one or two characteristic length scales included.

Patankar [36] showed that double (or multiple) roughness structures or slender pillars help in amplifying the apparent contact angle. The calculations presented are useful in fabricating surface geometries with self cleaning nature and can be generalized for surfaces with multiple roughness structures. This theory was found to be applicable at millimeter and smaller length scales but not for length scales of the order of nanometers. This theory was validated against previous experimental results [11, 37-39]. The theory further helps in making the heterogeneously wetted drop on a surface energetically more favorable.

Dupuis and Yeomans [40] used a lattice Boltzman approach to solve the equations of motion describing the dynamics of a drop on a topologically patterned substrate viz. an array of poles in this case. At a given size, surface tension, contact angle, and viscosity, the approach is found to be helpful in simulating the dynamic and equilibrium properties of a drop. In particular, it was well suited in understanding the behavior of an evolving drop.

Patankar [41] also studied the transition of a higher energy Cassie drop to a lower energy Wenzel drop. An energy barrier was observed to be present between the two states that need to be overcome by decreasing the gravitational potential energy during the transition. The best estimate for an energy barrier was considered to be an intermediate state where water fills the grooves below the contact area of a Cassie drop but the liquid-solid contact was yet to be formed. Though the Wenzel drop was known to be of a lower energy state, the transition was observed to occur only on overcoming the energy barrier, which is argued to not exist for all roughness geometries, a discussion consistent with the work of Marmur [42].

2.4 Thesis Objective

Wettability of solid surfaces is an important physical phenomenon and it has been known that surface topography plays a major role in the hydrophobic behavior of the surfaces. Much literature has concluded that heterogeneous wetting enhances hydrophobic nature due to increased drop mobility. However, in the present work, the question is: under what conditions is Cassie theory applicable?

It has been believed for a long time that the area void fraction, f , defined as the ratio of liquid-air contact area to the total projected surface area, is the primary determinant of the contact angle in the Cassie-Baxter state. In other words, two surfaces of varying roughness characteristic length scales but of the same area fraction would yield the same contact angle with the drop in the Cassie state. However, as it has been demonstrated herein by experimental measurements of advancing contact angle on structured hydrophobic surfaces, other parameters such as the characteristic length scale itself and more importantly, the continuity or discontinuity of the three-phase contact line topology are also determinants of the apparent contact angle and the hydrophobic nature of the drop.

CHAPTER 3

EXPERIMENTAL APPROACH

Wettability is characterized by the contact angle that the liquid drop makes with the surface under study. Many techniques have been developed to measure this contact angle. The present chapter outlines the experimental procedure employed to characterize the Wettability characteristics in this study as well as the procedure for fabrication of the specimen surface.

3.1 Chemicals and Materials

In the current study, surfaces of varying structured “roughness” were fabricated on a silicon wafer using a wet-etch photolithographic process. The roughness was introduced either as periodically placed square poles or square holes of varying characteristic roughness length scale ‘a’, viz. side of the square feature, and of varying area void fraction, f (See Figure 3.1a and Figure 3.1b for SEM images of two of the specimens with “holes” type and “poles” type roughness). A lithographic mask of various specimens (varying ‘a’ and f) was created. The fabrication process was performed as follows:

First, a 3” diameter <100> silicon wafer was cleaned using RCA1 and RCA2 cleans. Then, OCG-825 positive photoresist (Arch Chemicals, Inc.) was spin-coated at 3000 rpm for 40s with a ramping rate of 200rpm/s. to obtain a 0.9 μm thick film. After soft baking at 95°C for 30 minutes in a convection oven (National Compliance Company,

Model 5831), a contact aligner MJB3 (Karl Suss, Germany) was used to expose the photoresist with a dose of 25 mJ/cm² at 405 nm exposure wavelength.

This step was followed by developing (OCG Developer 934, diluted 2 parts of developer, one part of water for 65 seconds) and hard baking at 120°C for 30 minutes in a convection oven (Fisher Isotemp Oven 200 Series Model 215F). The whole wafer was then etched using the DRIE process in an Alcatel AMS 100 I-speeder Deep Reactive Ion Etching (DRIE) system. There were two different recipes used for two different etch depths: For the 30 μ etch depth, the following recipe was employed: surface temperature 10°C, helium pressure 8.0 mbar, source power 1800W, gasses: SF₆-300 sccm for 7 seconds, C₄F₈-150 sccm for 2 seconds, etch time: 6 minutes 40 seconds. For the 3 μ etch depth, the following recipe was employed: surface temperature 10°C, helium pressure 8.0 mbar, source power 1500W, gasses: SF₆-200 sccm for 2 seconds, C₄F₈-150 sccm for 1 second, etch time: 1 minute 40 seconds. The depth of the holes or the height of the poles, H, was also included in the study as a parameter such that H/a is varied between 0.03 and 1. The etch depth, H was controlled by varying the exposure time to the etch solution as mentioned above. Finally, the specimens were rendered hydrophobic by a silanization process identical to that used by Oner and McCarthy [4]. Here, the wafers were placed in a solution of ammonium hydroxide, hydrogen peroxide, and water (4:1:1) for 15 min, rinsed in copious amounts of water and spin dried. Then they are cleaned by submersion into a mixture of concentrated sulfuric acid and hydrogen peroxide (30%) in the ratio 7:3, overnight. The wafers were then cleaned with copious amounts of water and dried in an oven at 120°C for 2 hours immediately prior to silanization. The samples were then placed in a flask containing 0.5ml of organosilane reagent: heptadecafluoro-1, 1, 2, 2 –

tetrahydro -decyldimethylchlorosilane (FDDCS). Most of the widely used organosilanes have one organic substituent and three hydrolysable substituents. Reaction of these silanes involves four steps (see Figure 3.2). Initially, hydrolysis of the three labile groups occurs. Condensation to oligomers follows. The oligomers then hydrogen bond with OH groups of substrate. Finally during drying, a covalent linkage is formed with the substrate with concomitant loss. These reactions can occur simultaneously after the initial hydrolysis step with water. The reactions were made to take place in vapor phase which were carried out for 3 days at 65-70°C. The hydrophobized wafers were rinsed with toluene (two aliquots), ethanol (three aliquots), 1:1 ethanol/water (two aliquots), water (two aliquots), and ethanol (two aliquots) and then water (three aliquots), respectively and were dried in a clean oven at 120°C for 30 min. The resulting wafers had a self-assembled monolayer of the organosilane reagent on the silicon wafer.

3.2 Contact Angle Measurement

The advancing contact angles of a water drop on these samples were measured using a dynamic contact angle analyzer employing the captive needle technique (see Figure 3.3 for a typical drop demonstrating ultrahydrophobic behavior). The major components of the contact angle goniometer (Figure 3.4) are (1) a camera mounted on a traverse with three degrees of freedom along with a backlight for capturing high contrast images of the water drop, (2) a syringe pump that helps in creating a water drop of a precise volume and at the required rate (3) a computer for image acquisition, edge detection, and analysis. The goniometer is mounted on a table, free from vibrations and

leveled. The precision syringe pump was connected to a glass microneedle that was hydrophobized by silane treatment. The syringe pump was initially filled with deionized water. Traditionally, it was ensured that there were no air bubbles trapped in the tubing. Deionized water was pumped through the glass microneedle until a pendant drop was formed at the tip of the needle. Owing to the hydrophobic nature of the needle (low attraction force between water and the needle), the pendant drop is relatively small (less than 500 micron diameter) before it separates from the needle. Prior to the drop separation from the needle, the silanized silicon specimen whose dynamic contact angle needs to be characterized is gradually raised until the drop is sessile on the specimen. At this point, the syringe pump is turned on and water gradually injected into the sessile drop. For the formation of a Wenzel drop (grooves are filled with water), the distance between the surface and the needle is increased so that the pendant drop falls on the surface due to gravity and flushes the air out of the grooves, thus filling the grooves. The needle is brought back in touch with the drop and the water is gradually injected into the drop. As water is constantly being injected, the drop size increases. High resolution static images of sessile drop shape are obtained at predetermined time intervals by the automated image acquisition system with the drop being backlit.

The images are analyzed offline to calculate the drop contact angles, the contact circle diameter and drop volume using a MATLAB program. This program is capable of reading in an image file and calculating the drop edge using the Sobel method. An ellipse is then fitted to the drop shape. The points where the drop is sessile on the surface are manually identified. This process was not error-prone, as the drop reflection aided in this process. Finally, the tangent to the ellipse at the three-phase contact line is calculated to

output the contact angle which is defined as the angle between the tangent and the surface (Figure 3.5). The contact angle measurement process was validated by three procedures. Firstly, a solid steel ball with a flat bottom was used in place of the drop. A backlit image of the steel ball obtained was analyzed using the same MATLAB program to calculate the contact angle. This value was verified against an independent measurement of the contact angle on the steel ball obtained using a profile gage to ensure that the absolute error was less than 0.5° . The second verification was against data from Oner and McCarthy on plain silanized surfaces. The contact angles obtained in the current study were within 3° and were systematically less than the angles obtained by Oner and McCarthy. This difference could be attributed to the fact that the silanization procedure could have resulted in a slightly lesser area coverage fraction by the silane monolayer on the current specimen than those of Oner and McCarthy [4]. Finally, the advancing contact angle measurements were repeated on various specimens up to seven times on each specimen. The resulting data was analyzed for repeatability and reproducibility. The uncertainty in the advancing angle for all the cases presented herein was less than $\pm 1.5^\circ$.

The measured contact angles were compared to Cassie theory where the Cassie contact angle, θ_r^c is calculated from Equation (1.5). The variation of the contact angle with the area fraction, f and side of the square feature, a , is interpreted to understand the realm of applicability of the Cassie theory.

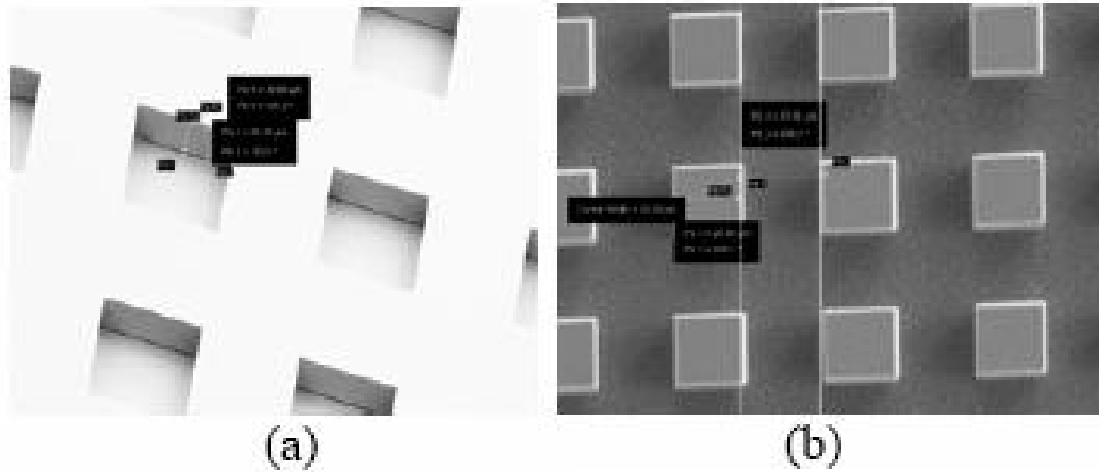


Figure 3.1 SEM images of the specimen with 'holes' and 'poles'

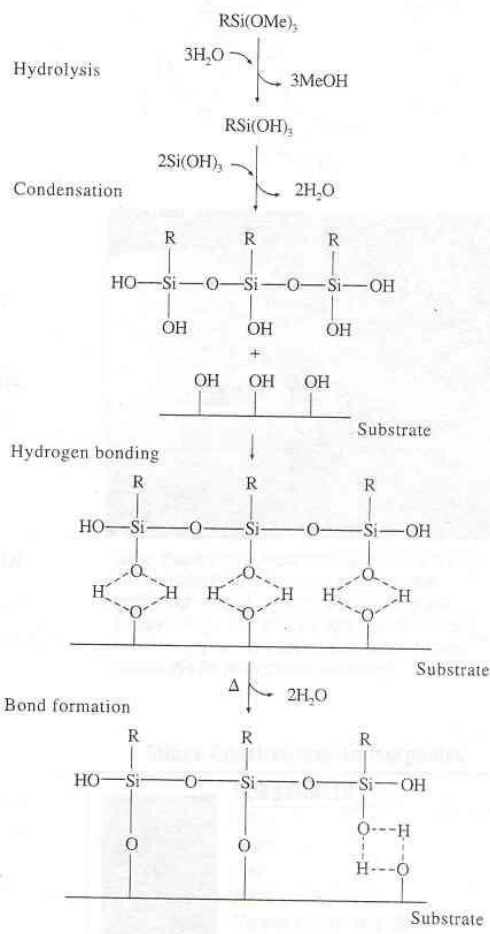


Figure 3.2 Hydrolytic depositions of silanes (courtesy: Gelest, Inc., manual)

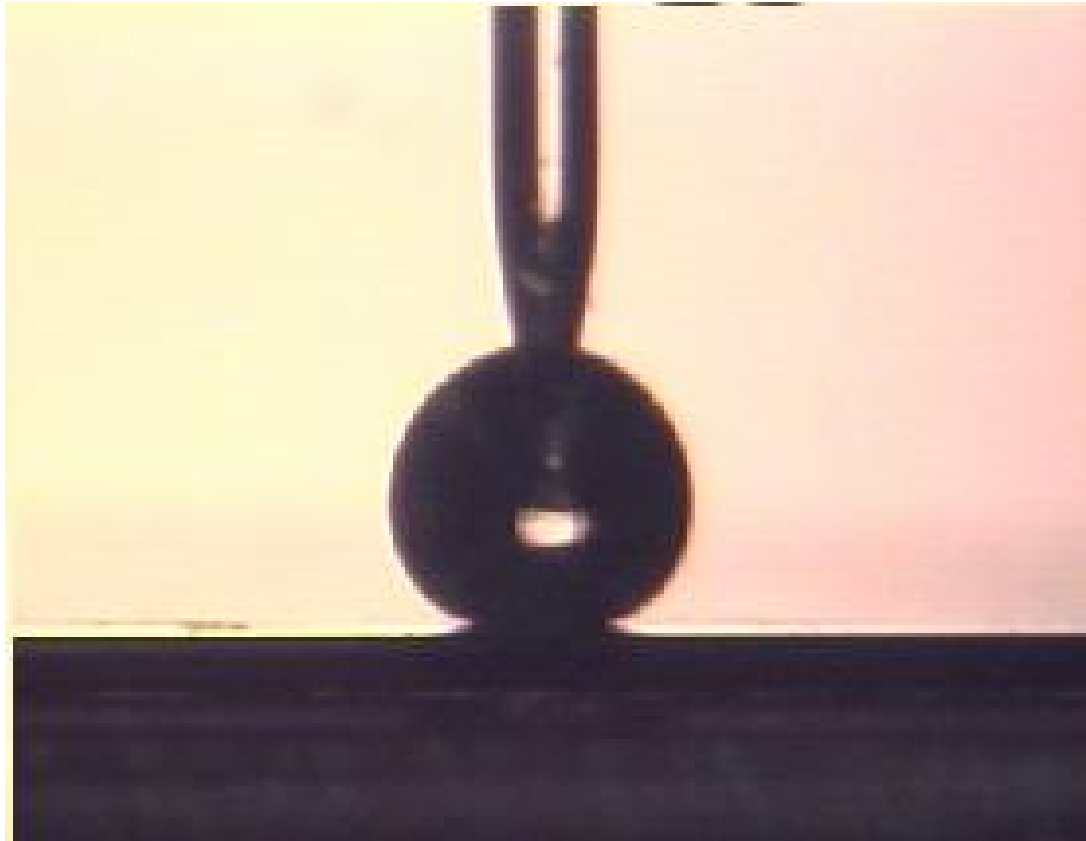


Figure 3.3 Image of a hydrophobic drop with the captive needle.

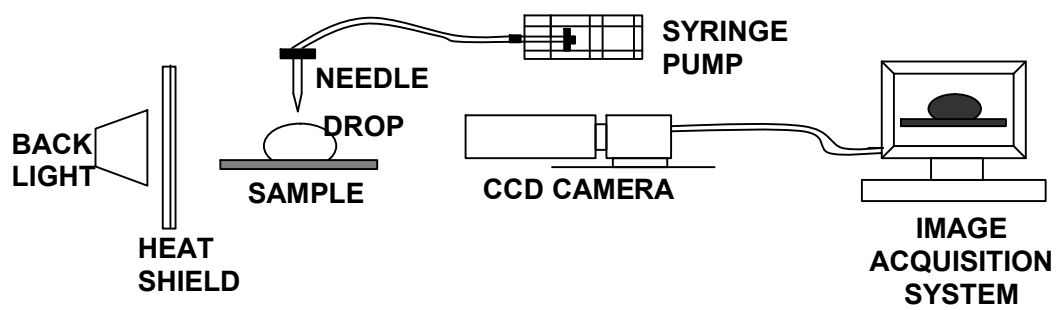


Figure 3.4 Contact Angle Goniometer.

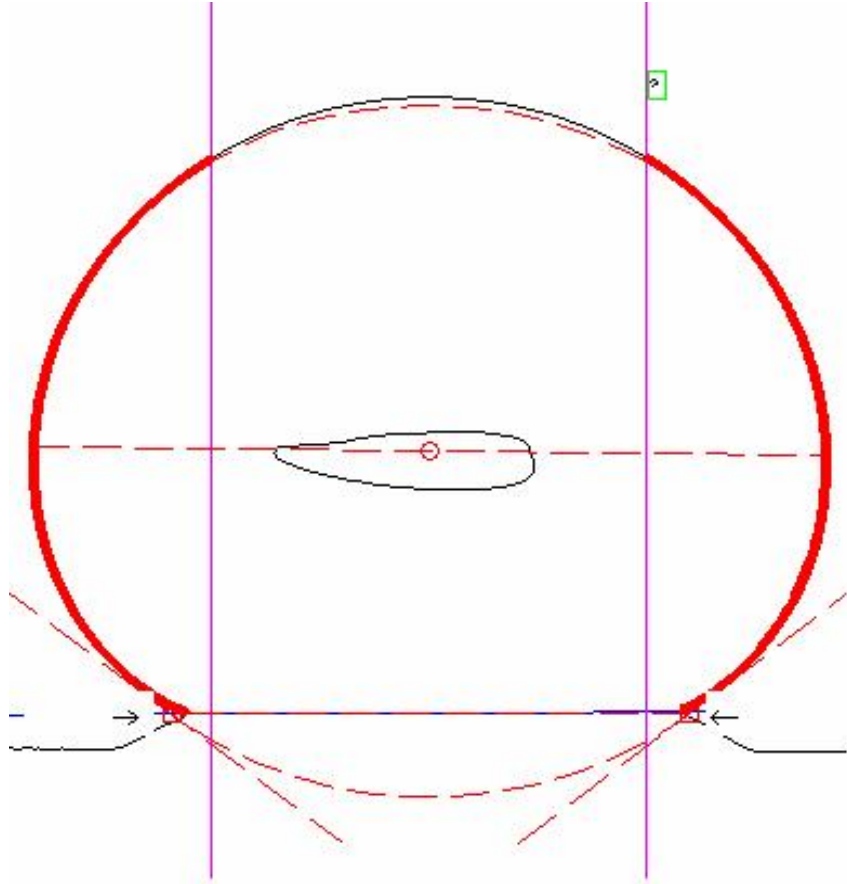


Figure 3.5 MATLAB program output

CHAPTER 4

RESULTS AND DISCUSSION

The dual stable states of existence of a water drop on a hydrophobic surface are the homogeneous (Cassie) and heterogeneous (Wenzel) states. Homogenous wetting is a regime where the liquid completely wets the solid surface, while heterogeneous wetting is defined as the case when the air (or liquid vapor) is trapped between the sessile drop and the surface.

The apparent contact angle in the heterogeneous wetted condition is given by the Cassie-Baxter theory [1] (see Equation (1.5)). According to these predictions, the area void fraction controls the resulting contact angle.

The apparent contact angle of the drop in the homogenous wetted condition, θ_r^w , is given by the Wenzel formula [2],

$$\cos \theta_r^w = r \cos \theta_Y \quad 4.1$$

where r is the roughness parameter defined as the ratio of the actual area of liquid-solid contact to the projected area on the horizontal plane. For the case of square poles of side 'a' and separated by a distance 'b' at the centers, this is given by

$$r = \left(1 + 4f \frac{H}{a} \right) \quad 4.2$$

with f being the area void fraction.

The advancing contact angles on various specimen surfaces were studied as a function of area void fraction and characteristic length scale, 'a' in the case of Cassie wettability and as a function of roughness parameter, r in the case of the Wenzel wetted

state. This chapter discusses in detail these results and by their help emphasizes the importance of the three-phase contact line behavior that has been hypothesized by researchers like Extrand [47] and Gao and McCarthy [48] in recent papers.

4.1 Heterogeneous Wetted State Results

Figure 4.1 and Figure 4.2 are graphs of the *advancing contact angles* versus *area fraction, f* , for hole depth (or pole height), $H = 30\mu$ and $H = 3\mu$, respectively, for $20\mu < 'a' < 100\mu$. For example, here $a=20H$ corresponds to data on 20μ square hole specimen, while $a=100P$ correspond to 100μ square pole specimen. The solid symbols correspond to data from 'poles' while the open symbols correspond to 'holes'.

It can be observed that, for periodically placed poles of size 'a', the advancing contact angle of the water drop increases with increase in the area fraction. The experimentally measured advancing contact angles are compared against predictions by the Cassie-Baxter theory in the same figure (see solid line in Figure 4.1). The Cassie-Baxter theory predictions were calculated from Equation (1.5), using the advancing contact angle for the smooth silanized specimen which was measured to be 103° . It must be mentioned that even though Equation (1.5) was derived using θ_Y , the thermodynamic contact angle, it has been widely used successfully with θ_a , the advancing angle [23]. It can be seen from the figure that the periodically placed poles follow the Cassie theory with the contact angle increasing with increasing area void fraction. The comparison between Cassie-Baxter theory and the advancing angle data in this figure results in a

correlation coefficient R^2 better than 0.9. Such correlation with the Cassie-Baxter theory for poles has also been reported by other researchers in the literature [8, 38].

The data presented in Figure 4.1 represent advancing contact angle measurements that were performed on samples with similar area void fractions and characteristic roughness length scales but varying in the three-phase contact line topology. For the purpose of this discussion, we define the three-phase contact line as comprising of the set of points which are in contact with air, liquid, and solid. In the case of the specimen where the drop was sessile on a surface with square poles, the set of points forming the three-phase contact line is discontinuous, in effect amounting to loops around the edges of the tops of the square poles. For this case, an “apparent” advancing contact line is however noticeable from macroscopic images. This apparent contact line is formed by the sharp crease created on the liquid drop surface at the points where the drop detaches itself from the substrate. The advancing dynamics of this apparent contact line have been hypothesized by Gao and McCarthy [49] to include rolling and ‘tank-tread’ motion during the process of wetting new poles on the surface. In the case of surfaces with poles, the drop is supported on a finite number of poles. As drop volume increases, the “apparent” contact line is hypothesized to experience tank-tread like motion and involves the addition of new poles underneath the drop.

However, for the specimens with square holes, the contact angle is seen to be independent of area void fraction in Figure 4.1. Furthermore, it can be observed that for a constant characteristic length scale, the contact angles for the specimens with square holes are greater than those of poles over the range of area void fractions investigated. For the case of a sessile drop on a surface with square holes, the three-phase contact line

at which the advancing motion occurs is continuous. This could possibly be occurring due to two reasons: (i) Cassie-Baxter theory does not distinguish between poles and holes structures. Therefore, this observed difference in the contact angle behavior could be attributed to the fundamental difference in the three-phase contact line topology – continuous in the case of the square holes versus discontinuous for the case of the square poles. (ii) The air trapped in the holes could be responsible for reduced wetting of the insides of the holes due to compressibility causing an increased macroscopic contact angle

For smaller pole height $H = 3\mu$ (Figure 4.2), there is a slight decrease in the overall values of the contact angles as compared to those observed for $H = 30\mu$. This is likely due to a partial Wenzel type wetting where the drop touches the bottom of the space between the poles or the holes. This is supported by the observation that this effect is more pronounced at higher ‘a’ values. In addition, the data for poles type surfaces follow the qualitative trend indicated by Cassie-Baxter theory. The data for holes however are in qualitative contradiction with Cassie-Baxter theory in that the contact angle a surface with square holes decreases with increasing area void fraction, f for a constant ‘a’. This can be attributed to the fact that as f increases, the center spacing between the holes increases, thereby increasing the chance of Wenzel type wetting behavior. Furthermore, the partial Wenzel effect is more significant for the poles than the holes. This is again reasonable since the holes support the drop on all sides whereas the poles do not. The drop will sag to the bottom of the space between the poles more easily than into the cavity of a hole.

Figure 4.3 and Figure 4.4 are plots of the *advancing contact angle* versus *roughness length scale* 'a' for $H = 30\mu$ and $H = 3\mu$, respectively. For example, here $f=0.25H$ corresponds to data on 0.25 area void fraction square holes specimen, while $f=0.75P$ correspond to 0.75 area void fraction square poles specimen. The solid symbols correspond to data from 'poles' while the open symbols correspond to 'holes'.

It is evident from these figures that, as the value of 'a' increases, the contact angle for the poles increases initially and then decreases. This trend is particularly more pronounced in Figure 4.4 with the solid symbols which correspond to poles. From this trend we can conclude that there is an optimal value of 'a' at which the angle becomes maximum and that a sample with lesser value of 'a' results in a decrease of contact angle. The decrease in contact angle for poles type surfaces with decreasing 'a' for values greater than $20\mu\text{m}$ can be explained by the fact that the spacing between the poles has to increase to accommodate an increase in area void fraction. This results in partial wetting between the poles which causes a slight decrease in contact angle owing to Wenzel theory. For holes however, the contact angle is found to be independent of 'a'. It can also be seen from comparing the graphs in Figure 4.3 and Figure 4.4 that the contact angle increases with increasing depth. This is again a result of the reduction in Wenzel-type behavior at larger etch depths.

Receding contact angles were measured on the 30μ specimen by heterogeneous wetting. CAH was calculated as the difference between the advancing and receding contact angles. Figure 4.5 and Figure 4.6 are plots for the CAH versus area void fraction and characteristic length scale, respectively. These figures show the consistency with which the surfaces with holes have higher CAH in comparison with surfaces with poles.

For the case of holes, the defect pinning force or increase in the area number density of the defect sites increases the difference between the thermodynamic and advancing contact angles, thus resulting in higher CAH.

4.1.1 Summary

The contact angles were measured on specimens with $H = 30\mu$ and $H = 3\mu$ and their sensitivities to area void fraction and characteristic length scale, 'a' were studied. The contact angles for the specimen with $H = 30\mu$ were found to be greater than those on the 3μ specimen. The contact angles on the specimen with poles varying with area void fraction were observed to follow the Cassie-Baxter predictions as reported in literature. There existed an optimum value of 'a' at which the contact angle was the highest. The contact angles were further observed to decrease on increasing the characteristic length scale 'a', owing to the partial Wenzel drop formation. The contact angles on specimens with holes were observed to be higher than those for specimens with poles. They also contradict the Cassie-Baxter theory and are independent of area void fraction and 'a'. This may be attributed to the fact that the three-phase contact line is continuous in the case of holes and discontinuous in the case of poles. The CAH was calculated and found to be consistently higher for the case of holes.

4.2 Homogenous Wetted State Results

Figure 4.7 and Figure 4.8 are graphs of the *advancing contact angles* versus *roughness parameter, r*, (given by Equation (4.2)) for hole depth (or pole height), $H=30\mu$ and $H=3\mu$, respectively. The solid symbols correspond to data from ‘poles’ while the open symbols correspond to ‘holes’. The two specimens were tested for reproducibility. The uncertainty for 30μ and 3μ specimen was found to be 1.16% and 2.05%, respectively.

It can be observed from these figures that for the same roughness value the Wenzel advancing angles on the surfaces with holes are generally greater than those with poles. The reasons for this behavior may be two fold: (i) the three-phase contact line is continuous in the case of the square holes versus discontinuous for the cases of the square poles (ii) For the same force with which the drop was placed on the surfaces with holes and poles, the air remains trapped in the holes while it may have been flushed out in the case of poles. This may be responsible for reduced wetting of the insides of the holes due to compressibility causing an increased macroscopic contact angle.

Due to the second reason, Wenzel theory is assumed to best explain the surface with poles separated by 100μ length scale and of 75% area void fraction. This is observed to be true on both the $H = 30\mu$ and 3μ specimens (see the lowest angles in Figure 4.7 and Figure 4.8).

The contact angles for the 30μ etch depth sample are observed to be greater than those on the 3μ sample. The roughness parameter, r is calculated to be small on the 3μ sample as compared to the 30μ sample. For this surface with low pole height, there is a

greater possibility of achieving the Wenzel drop state for a constant force with which the drop is placed. The ease with which the poles (holes) of small heights (depths) can be wetted is the reason for achieving the Wenzel state for the 3μ sample.

Figure 4.9 and Figure 4.10 are graphs of the advancing contact angles measured on all the surface topologies versus the corresponding contact angles calculated from the Wenzel theory (using Equation (4.2)) for $H=30\mu$ and $H=3\mu$, respectively. The solid line in these graphs has a slope 1 and helps form a correlation between the measured and calculated angles i.e. a point lying on this line represents that a case where the measured and calculated angles are equal. The dotted lines represent the uncertainty associated with these measurements.

It can be seen from the graphs that the measured contact angles are greater than the calculated contact angles. According to the Wenzel theory, homogenous drop contact angle is achieved when the grooves of the poles or holes are completely wetted by the liquid. But in practice, the complete wetting of the grooves is not always achieved. By allowing the droplet to impact the surface from a certain height, we attempt to flush the air out of the grooves with the help of the impact drop momentum. But, if the air remains trapped, especially in the case of holes, the resulting advancing contact angles will be higher than the theoretically calculated angles from the Wenzel theory.

The five closest data points to the solid line were observed to be the contact angles on the surfaces of poles with 0.5 and 0.75 area void fractions and of different characteristic length scales, 'a'. In addition, the five points furthest away from the line were also observed to be that of holes with 0.25 area void fractions and different values of the characteristic length scales, 'a'. This clearly explains that the observed wetting

behavior is due to Wenzel theory. All the other contact angles are partially formed by the Cassie theory. Also, a majority of the contact angles measured on the 3μ sample are observed to be closer to the corresponding calculated values as opposed to the 30μ sample. This is attributed to a higher probability of achieving the Wenzel drop on these surfaces.

4.2.1 Summary

Contact angles were measured on specimens with holes and poles and with $H=30\mu$ and 3μ varying in area void fraction and characteristic length scales. Drops are placed from a certain height so that they fall on the surface with a force sufficient to flush out the air from the grooves, thus achieving the homogenous wetting condition. However, it was observed that this wetting state was not always achieved as air remains trapped especially for the surface with holes. Thus the contact angles measured on holes were observed to be higher than those on poles. Further, the majority of the angles obtained on the 3μ specimen were observed to be closer to the angles calculated from the Wenzel equation. This is understood to be due to the finer roughness for the 3μ sample, making it easier to wet the grooves for such small heights. Also, the Wenzel theory was observed to satisfy the predictions for specimen with greater area void fraction (0.75) varying in characteristic length scale 'a' and spacing between the holes or poles. It was difficult to achieve Wenzel angles for the cases with low area void fraction (0.25) owing to partial Cassie drop formation.

4.3 Discussion

The contact angles were measured on various specimens ranging in characteristic length scale as well as surface void fraction. Conventional Cassie theory [50] dictates that the area void fraction controls the resulting contact angle. This has also been substantiated by Gibbs free energy minimization arguments [39]. However, recent results from Extrand [15, 47, 51, 52] have questioned the validity of these results. He argues that contact angle behavior has to be governed by the three-phase contact line behavior more so than the total wetted area. In other words, the contact angle exhibited by the drop has to depend on the wetted void fraction in the vicinity of the contact line rather than underneath the drop where the liquid/solid area is static and unchanging. In addition, Gao and McCarthy [49] also explain that the dynamical contact angle behavior has to be governed by a one-dimensional phenomenon such as three-phase contact line.

The results from the current experiment further reinforces the theories proposed by Extrand [15] and McCarthy and co-workers [49]. As can be observed from Figure 4.1, the contact angles for “holes” specimens are relatively constant with respect to area void fraction whereas the contact angle for poles obeys the Cassie theory very closely. The fundamental difference between these two classes of specimens is that for the case of “holes,” the three-phase contact line is continuous, whereas for “poles,” the contact line is discontinuous. This clearly demonstrates the effect of contact line topology on contact angle.

de Gennes has proposed various mechanisms that cause the advancing contact angle to be different from the “thermodynamic” contact angle presented by Young’s equation. The main hypothesis that he proposed which has since been experimentally

validated for advancing drops on a smooth surface is the presence of defect sites on the surface that cause the drop contact line to be pinned. These defects could arise out of surface chemical heterogeneities, surface roughness or solutes in the drop. The density distribution of these defect sites dictates the degree of hysteresis exhibited by the drop. As either the defect pinning force or the area number density of the defect sites increases, the difference between the thermodynamic and advancing contact angles increases, thus resulting in increased contact angle hysteresis. In addition, as the drop advances on a surface of uniform area number density of defects, the total pinning force per unit length of the contact line reaches an asymptotic value which causes the advancing contact angle to reach an asymptotic value. Consider a sessile drop on a defect-free smooth surface. The contact angle under thermodynamic equilibrium is given by Young's equation (Equation (1.4)). This equation arises out of a force balance at the three-phase contact line between the forces due to solid-liquid, solid-vapor, and liquid-vapor interfacial attractive forces. On a real surface however, the drop is subject to a constant density and random distribution of defect locations. The pinning forces at these defect locations cause the three-phase contact line to be pinned to a smaller wetted circle radius on the surface for the same drop volume, than would be manifested under defect-free conditions, viz. Young's contact angle. For this condition, the actual measured advancing angle on a defect-free surface, θ_a is greater than θ_v and is attributed to the existence of a uniform external inward radial pinning force per unit contact line length, f_p . As the drop volume increases, the pinning force per unit length attains an asymptotic value due to the statistically large number of randomly distributed defect sites exerting their influence on the contact line. Under this condition, Equation (1.4) can be modified to include f_p to give

$$\cos(\theta_a) = \frac{\Gamma_{SV} - \Gamma_{SL} - f_p}{\Gamma_{LV}} \quad 4.3$$

Equation 4.3 can be rewritten as

$$\cos(\theta_a) = \cos(\theta_Y) - \frac{f_p}{\Gamma_{LV}} \quad 4.4$$

Now consider a sessile drop on a surface with either square or circular holes. There is an additional pinning force generated at the heterogeneities arising out of the sharp discontinuity in material properties on the surface, viz. solid surface and air. This additional pinning force per unit length f'_p will cause the contact angle to further be modified from the advancing contact angle measured on a plain surface. For this condition, Equation (4.4) becomes

$$\cos(\theta'_a) = \cos(\theta_a) - \frac{f'_p}{\Gamma_{LV}} \quad 4.5$$

where θ'_a is the advancing contact angle on the surface with holes.

We now discuss the case pertaining to a sessile advancing drop on a surface with square holes. Letting 'b' represent the center spacing between the square holes and 'a' the side of the square holes, the area void fraction is given by $f = a^2/b^2$. For the case of square holes, the vertices of the square holes represent potential pinning sites of the three-phase contact line. If the contact line is found to intersect one of the edges of a square holes, that configuration is not stable due to the local angle formed between the edge and the contact line, which causes the contact line to slide along the edge till it encounters a vertex. Therefore, the contact line will always remain pinned only at the vertices of the square holes. We numerically calculate the number of pinning defects per unit length of

the three-phase contact line by snapping an initially circular three-phase contact line to the nearest hole vertices (Figure 4.11a shows a schematic representation of this calculation before and after the pinning process). The numerical computation proceeds by moving all intersection points between the contact circle and the edges of the square holes to the geometrically closest vertex. For a drop exhibiting a three-phase contact line radius, R , where $R \gg b$, we find that the total number of defects through which a pinned contact line passes for a constant R , is proportional to R and *independent of the area void fraction*. Figure 4.12 shows the total pinning force per unit length of contact line for square holes. Here, the force per defect is assumed to be $7\text{E-}6$ N. As can be seen from this figure, the total pinning force per unit length f'_p is nearly independent of f . This is expected owing to the fact that in a surface area equal to b^2 , there are exactly four defects corresponding to the four vertices of the square hole of side 'a', independent of 'a' and therefore f . If the pinning force at each defect is equal, the total pinning force per unit contact line length is thus independent of area void fraction. Phenomenologically, this is the same reason why the advancing contact angle on a real surface with random and uniform defect distribution reaches an asymptotic value. It is therefore to be expected that the advancing contact angle will only depend on the area number density of the defects. Since the area number density of the defects is independent of f , the advancing contact angles measured on various surfaces with square holes is independent of f and 'a' as can be seen from Figure 4.1. In addition, it may be noted that if the area number density of the defects can be varied by introducing a cavity of a different shape (e.g. Pentagonal or star-shaped), the advancing contact angle is likely to be constant but different. In terms of the global free energy, each pinning defect may be viewed as introducing several

metastable minima. As the three-phase contact line advances from one defect to the next, the free energy changes from one metastable minimum to another. The above arguments only hold for surfaces where the point defect sites dictate the behavior of the three-phase contact line. In situations where edge defects are dominant, the results are expected to be different. A simple situation where edge defect pinning is important will be the case of *circular* holes. Numerical simulations of the contact line wrapping around 1-dimensional circular defects (schematically represented in Figure 4.11b before and after the pinning process) show that the fraction of the contact line in contact with the cavity edge is a monotonic non-linear function of the area void fraction f . Assuming that the total pinning force is proportional to the pinned line length, from Equation (4.5) the contact angle is a function of the area void fraction. We test the consequence of the above arguments by comparing with experiments conducted by Abdelsalam et al. [53] on advancing sessile drops on surfaces with circular holes.

Consider a sessile drop on a surface with a hexagonal arrangement of circular holes of radius ‘ a ’ arranged ‘ b ’ apart at centers. As shown schematically in the bottom image of Figure 4.11b, the actual contact line on this surface will form a continuous curve such that a part of it remains circular as though it were on a smooth surface and the rest of the contact line is pinned along the edges of the circular holes. If the pinning force per unit length of contact line circumscribing a circular cavity is η and if the fraction of the actual contact line length that is situated around the edges of the circular holes is ξ , the total pinning force per unit length on the advancing three-phase contact line is given by $f'_p = \xi\eta$. We have numerically calculated ξ for surfaces of varying area void fraction by allowing the three-phase contact line circle to be re-routed around the circular holes

which it intersects, satisfying a constraint that the total arc length around each circular cavity is minimized. Figure 4.12 is a plot of ξ versus area void fraction, f for surfaces with circular holes. As can be seen from this figure, ξ increases monotonically with f . Therefore, the pinning force f_p' is expected to have the same non-linear monotonic dependence on the area void fraction f . The pinning force dependence on f results in the advancing contact angle θ_a^* being a function of the area void fraction, as indicated by Equation (4.5).

Figure 4.13 is a graph depicting data from Abdelsalam et al. re-plotted with the Cassie-Baxter theory and the advancing angles predicted by Equation (4.4) for their surface geometry. For this case, η was chosen to be 0.105 N/m. The advancing angle measured by them on a plain thiol-modified gold surface, θ_a was equal to 70° . Figure 4.13 shows the experimental data of Abdelsalam et al. [53] compared the Cassie-Baxter theory and the present three-phase contact line pinning theory. While Abdelsalam et al. [53] compared their data with Cassie-Baxter theory, it is clear that the present theory fits the data to good accord. It must be concluded based on the physical arguments presented in this document that the favorable comparison between their circular cavity surface data and Cassie-Baxter theory may be somewhat fortuitous.

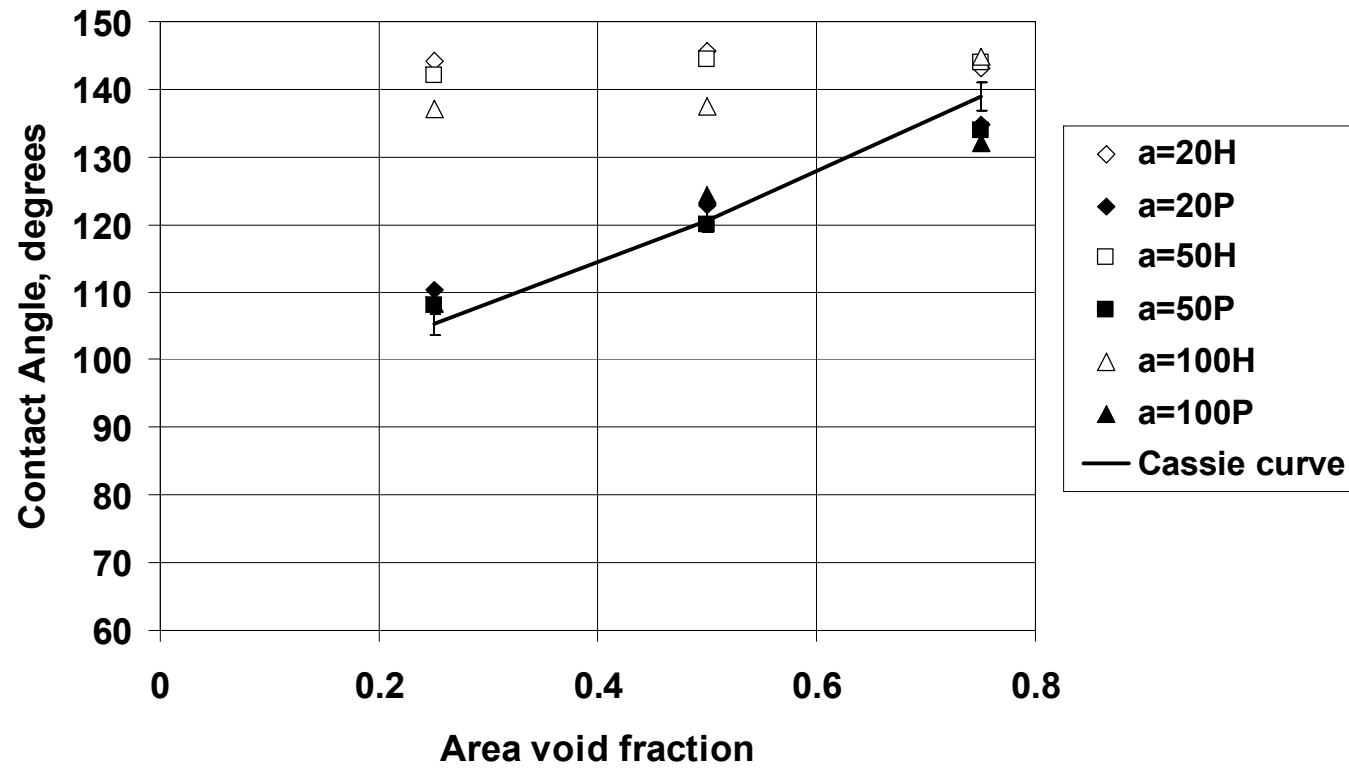


Figure 4.1 Contact angle versus area void fraction for varying characteristic length, 'a' (H=30 microns)

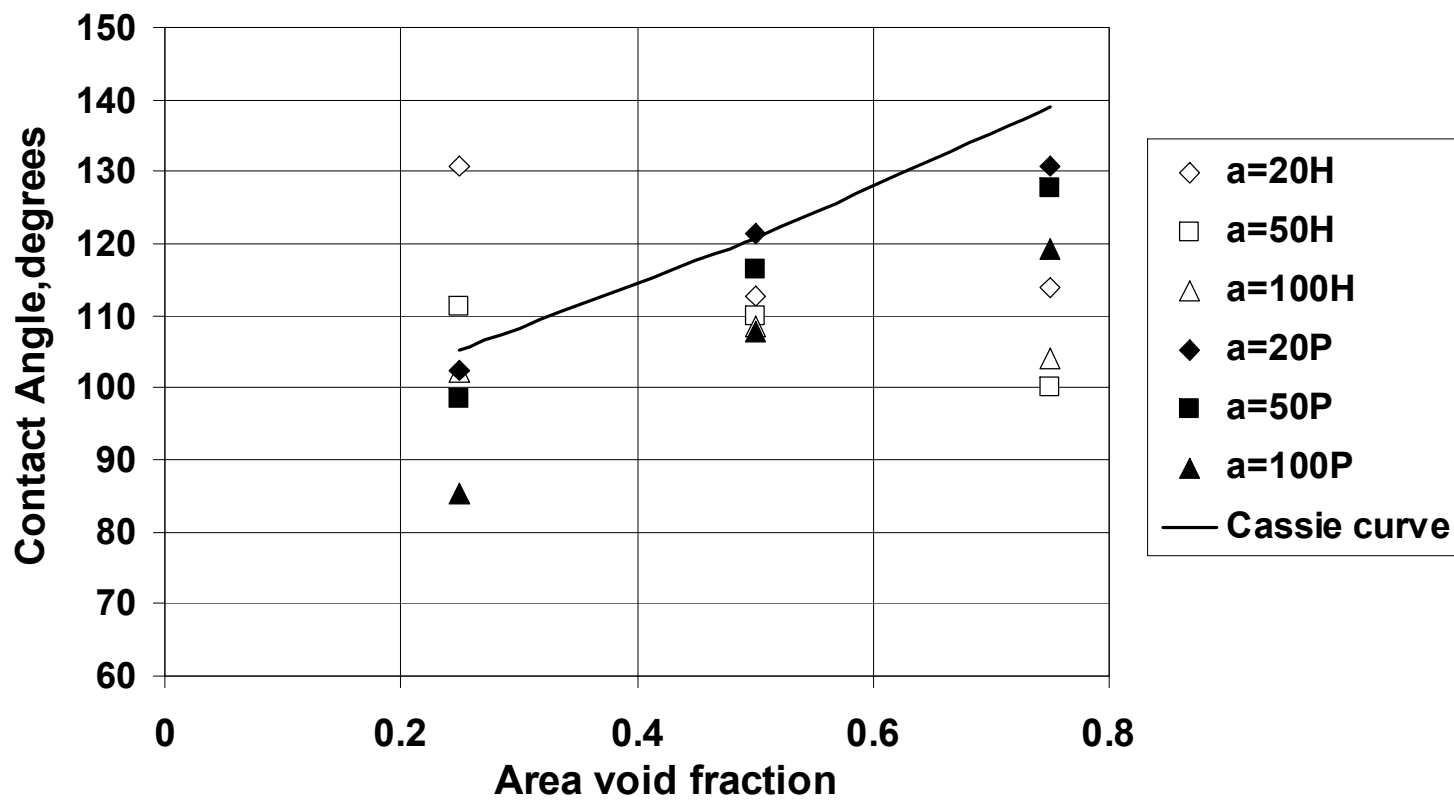


Figure 4.2 Contact angle versus area void fraction for varying 'a' (H=3 microns)

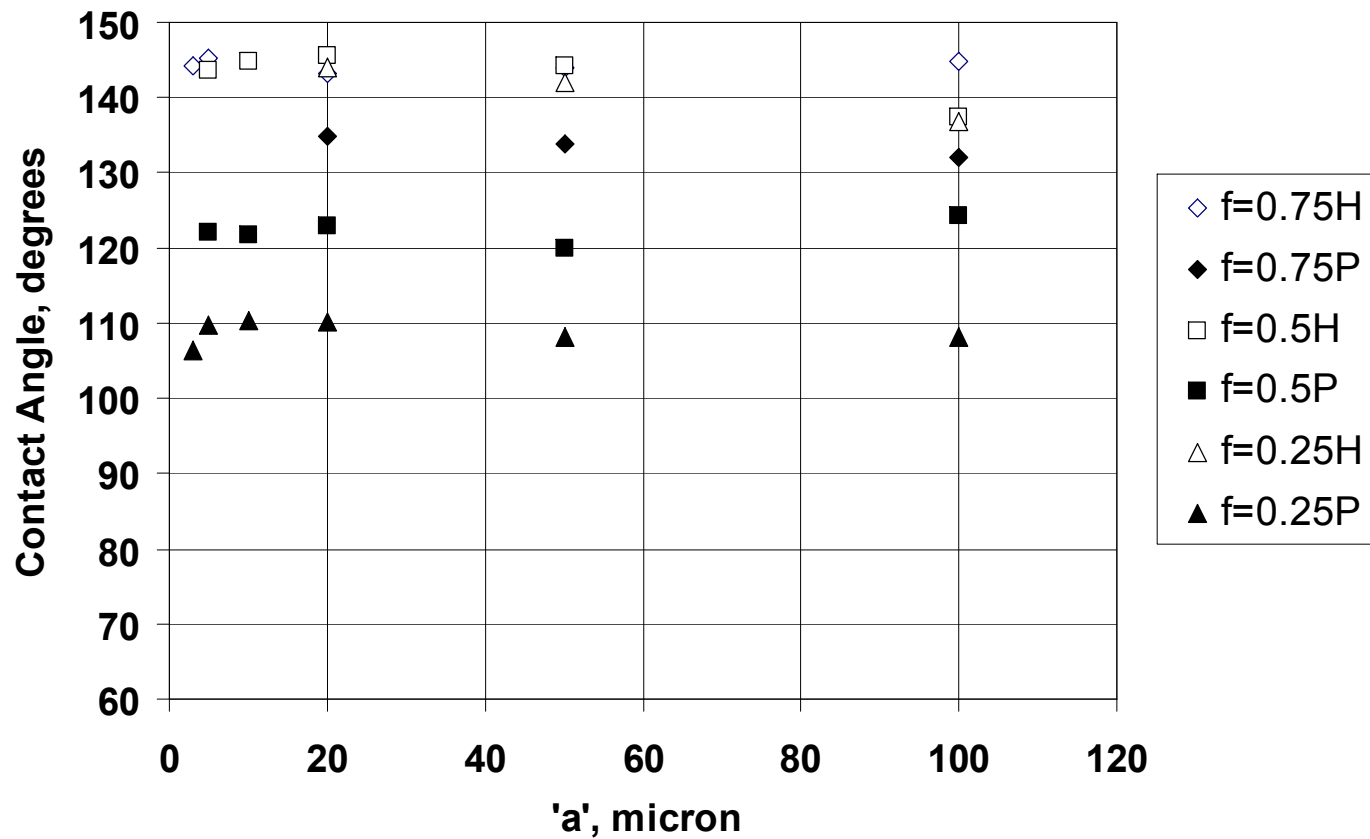


Figure 4.3 Contact angle versus 'a' for varying area void fraction (H=30microns)

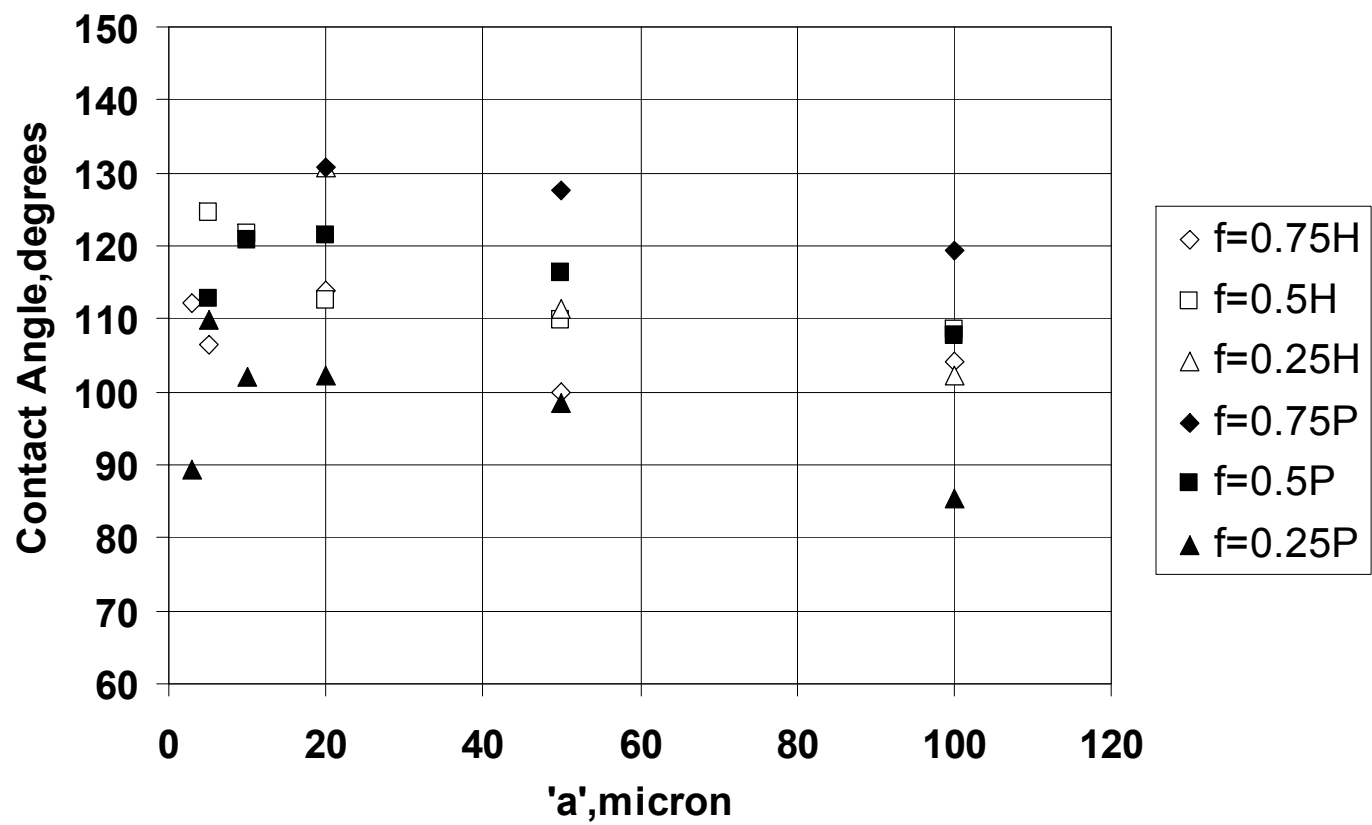


Figure 4.4 Contact angle versus 'a' for varying area void fraction (H- 3microns)

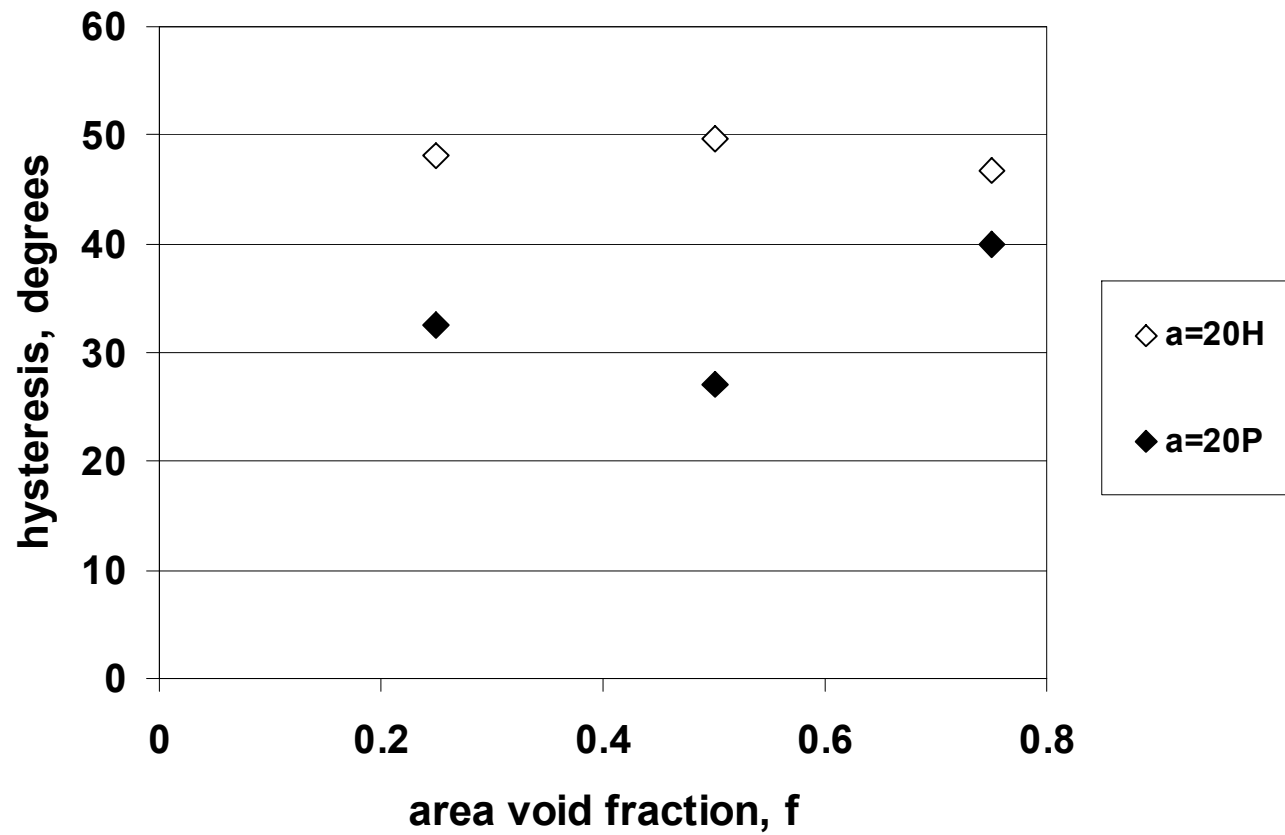


Figure 4.5 Contact angle hysteresis versus Area void fraction for characteristic length, 'a' = 20 microns (H=30 microns)

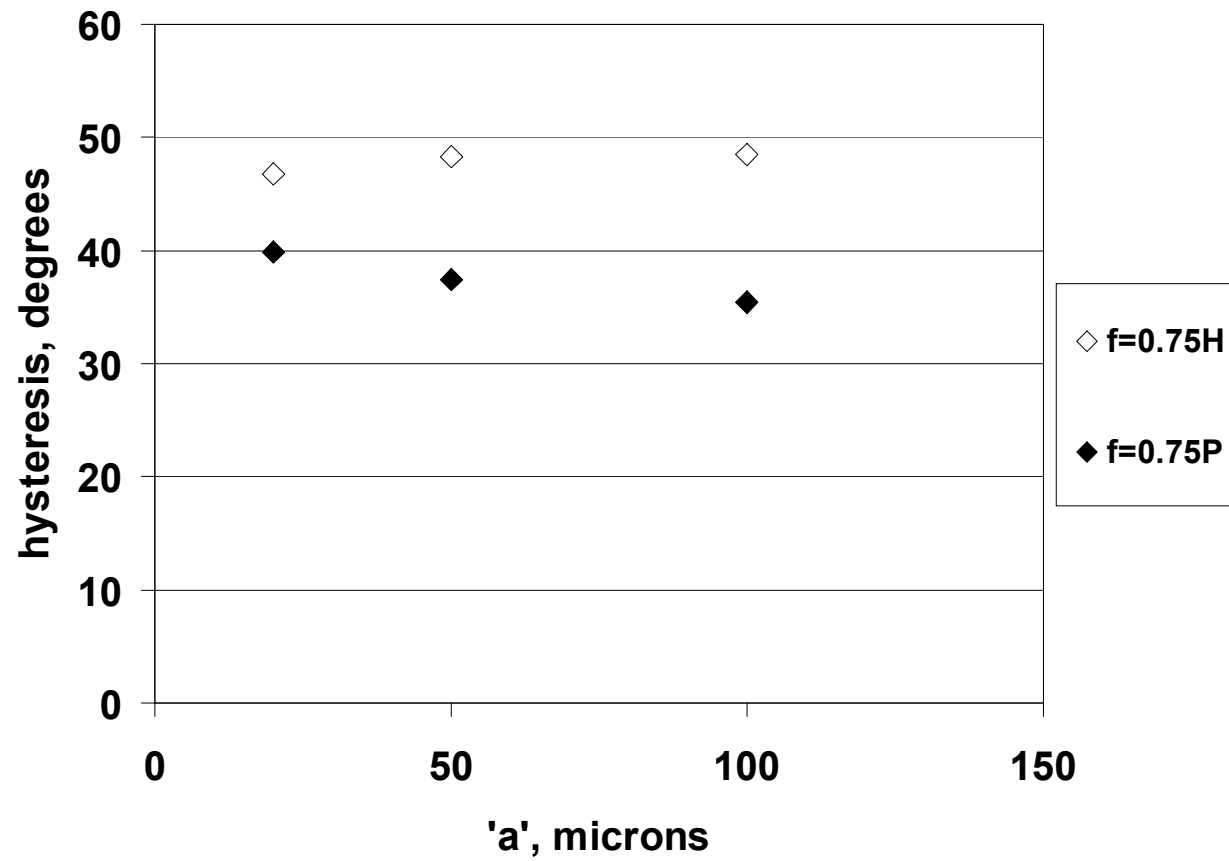


Figure 4.6 Contact angle hysteresis versus 'a' for area void fraction, $f=0.75$ ($H=30$ microns)

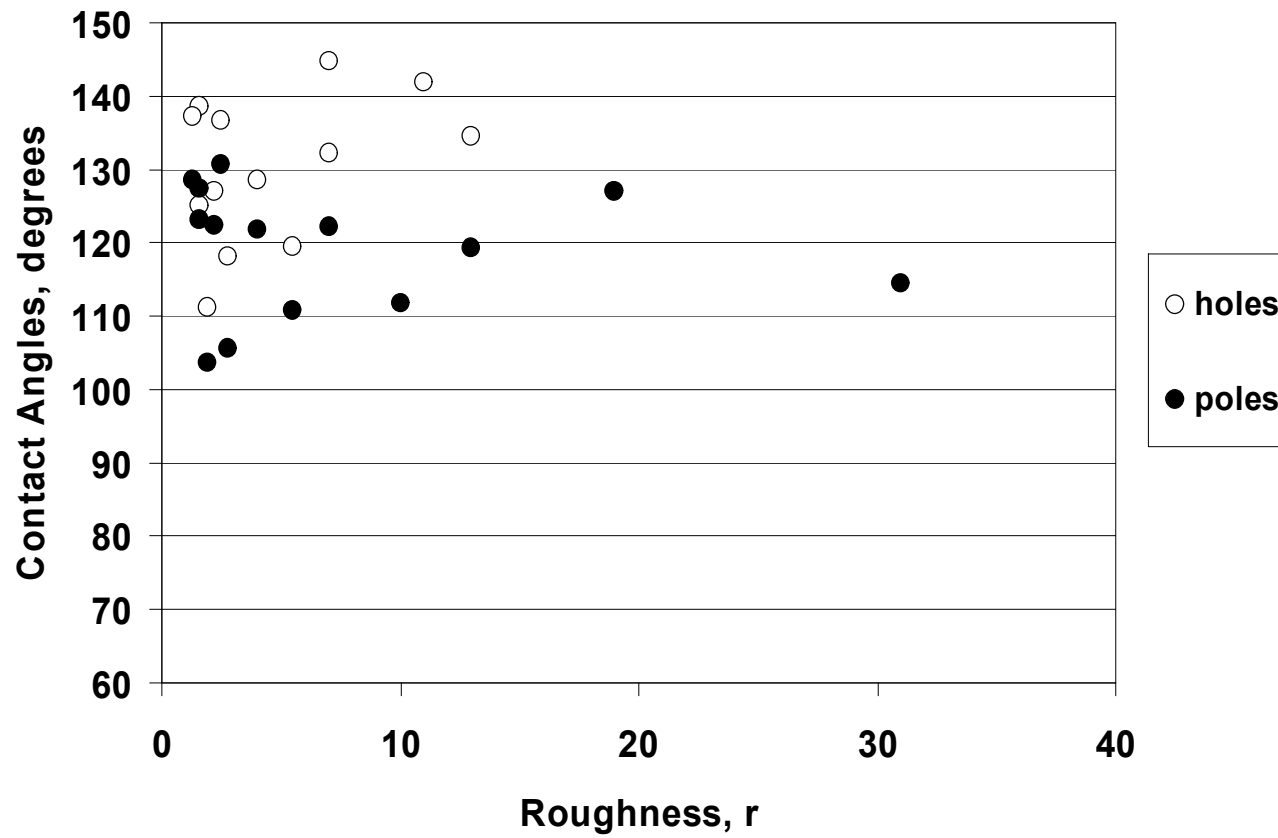


Figure 4.7 Contact angle versus roughness, r (H=30 microns)

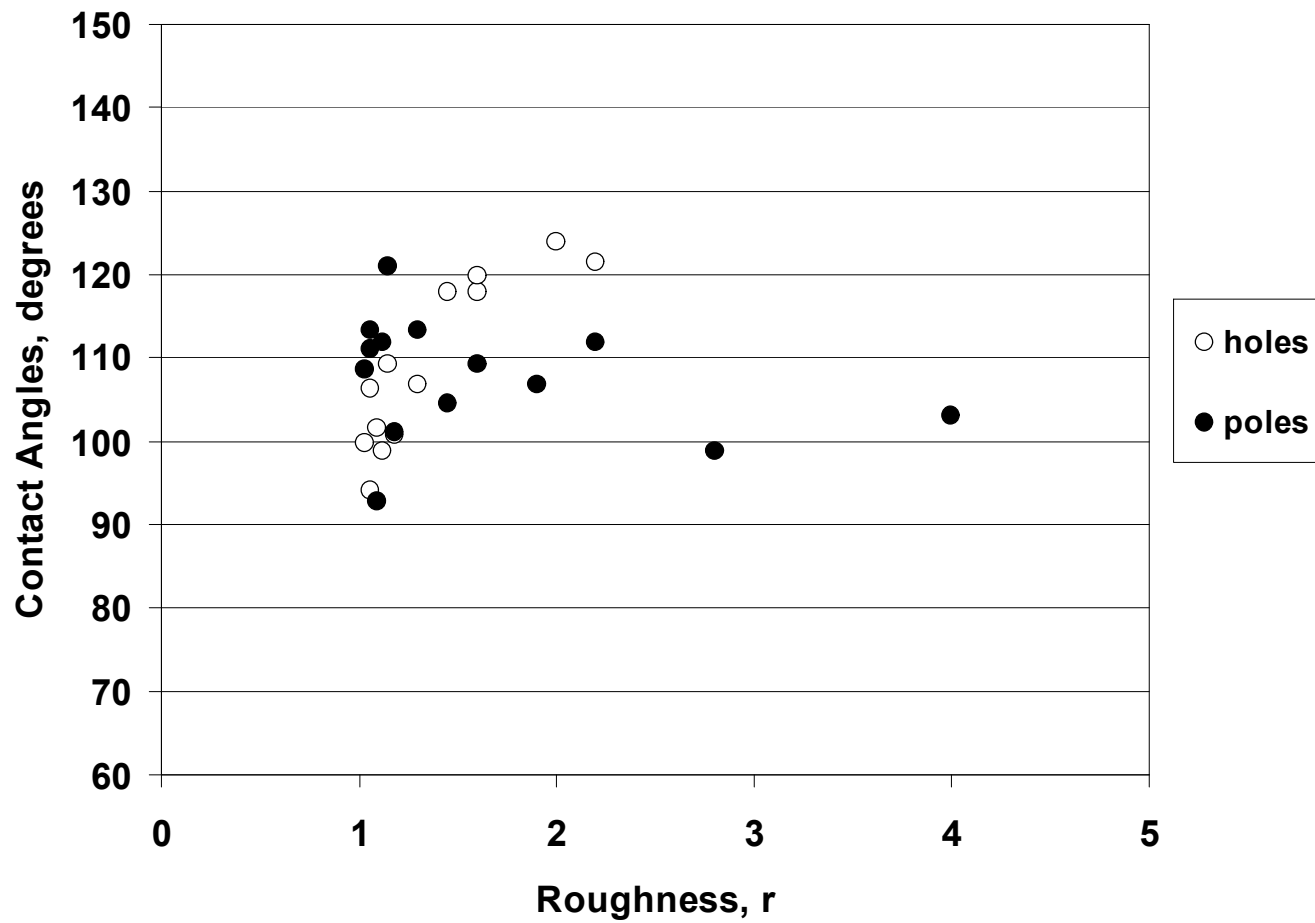


Figure 4.8 Contact angle versus roughness, r (H=3 microns)

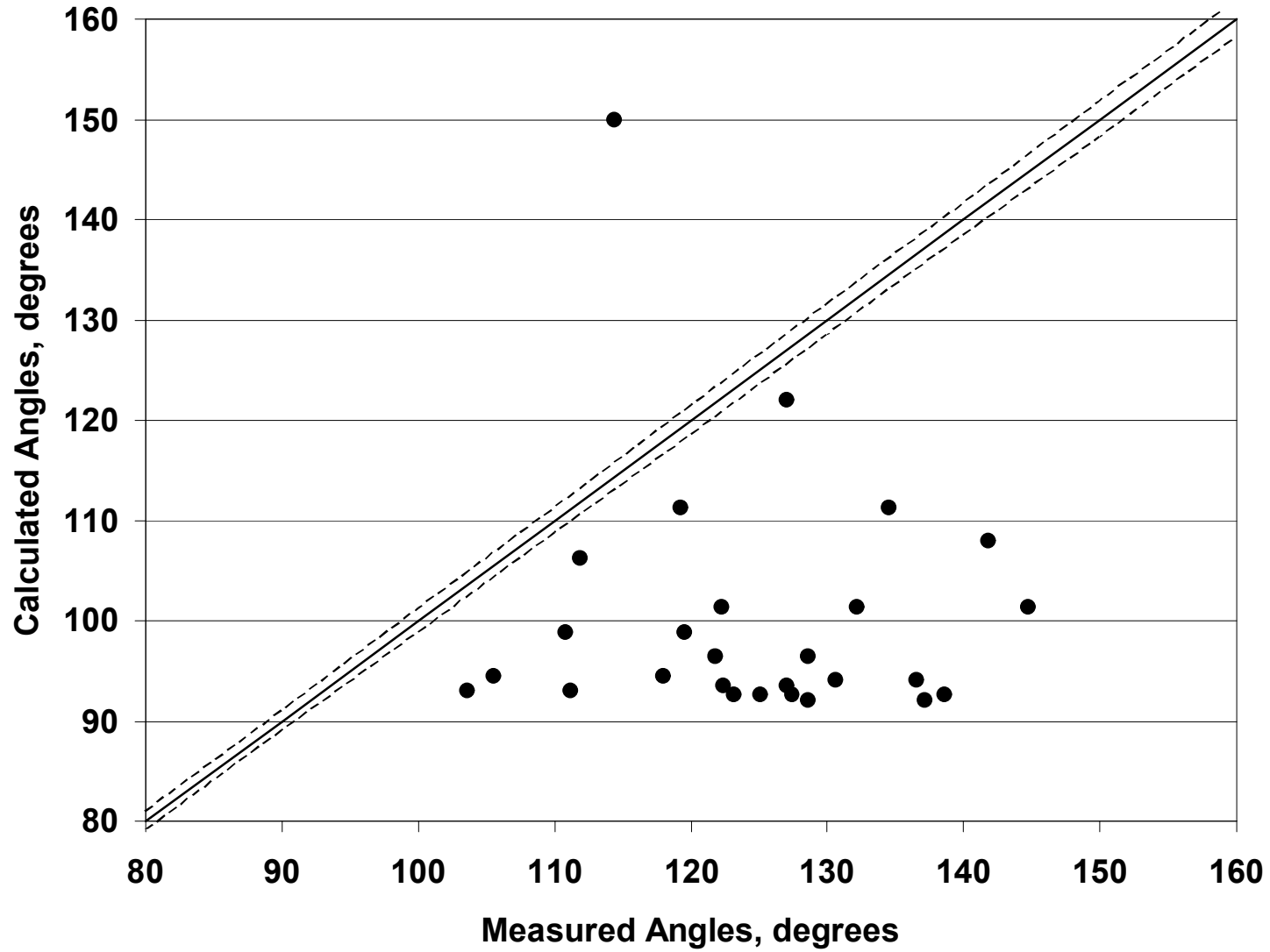


Figure 4.9 Measured contact angles versus calculated contact angles (H=30 microns).

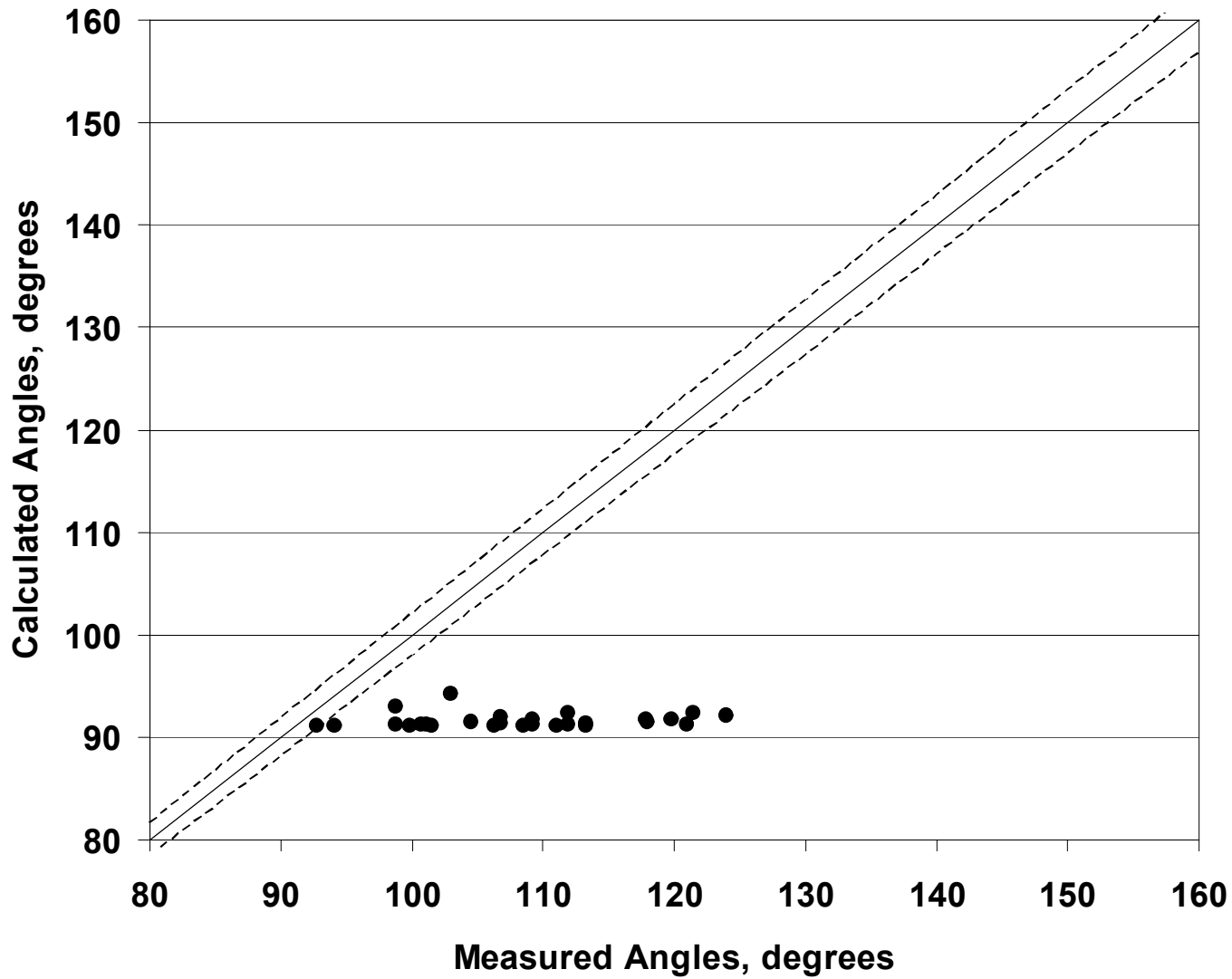


Figure 4.10 Measured contact angles versus calculated contact angles (H=3 microns)

Figure 4.11 Contact line on surface with square and circular holes. The images above depict contact circle before the pinning and the images below depict pinned contact line.

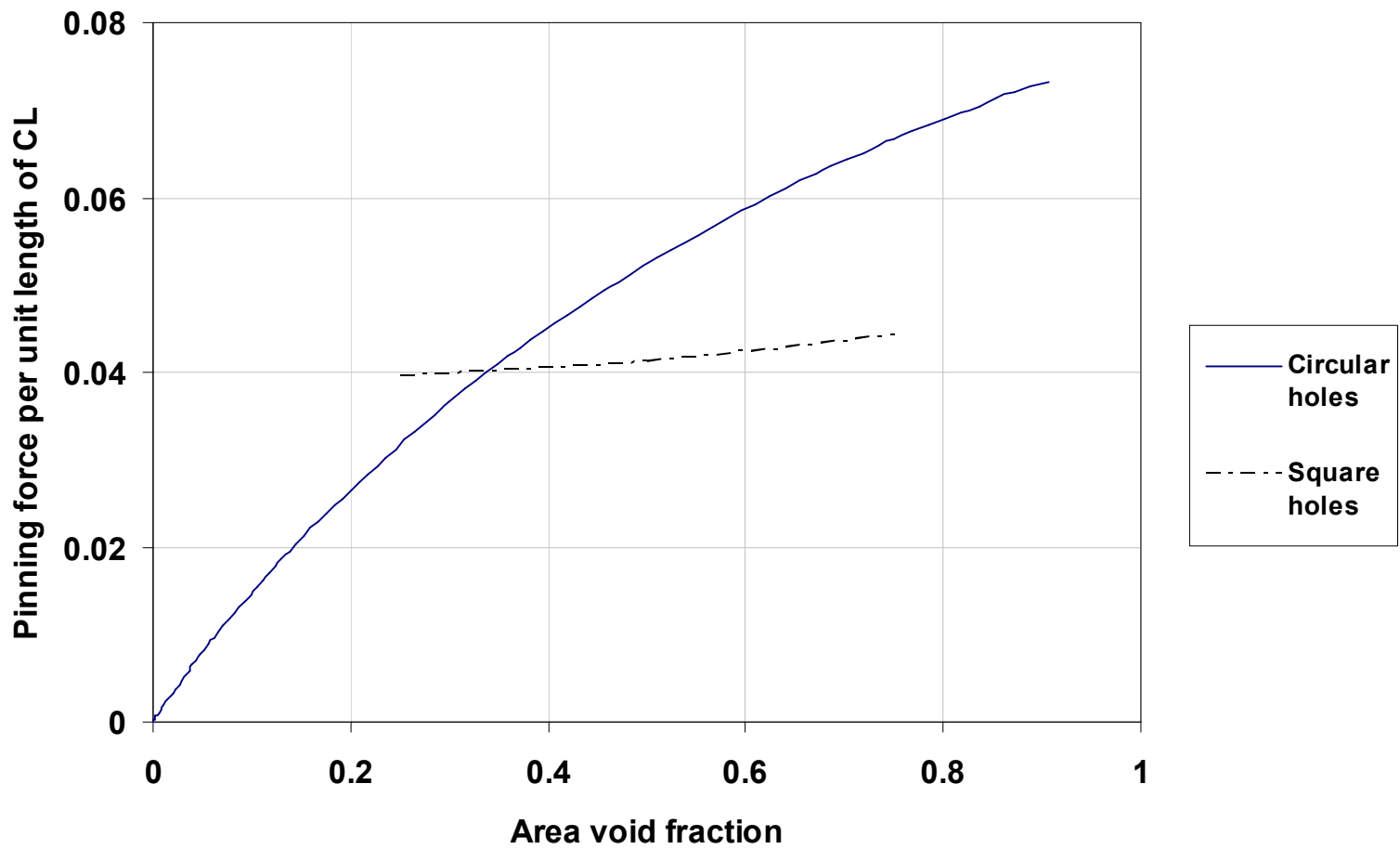


Figure 4.12 Pinning force per unit length of the contact line f_p' versus area void fraction, f for surfaces with circular and square cavities.

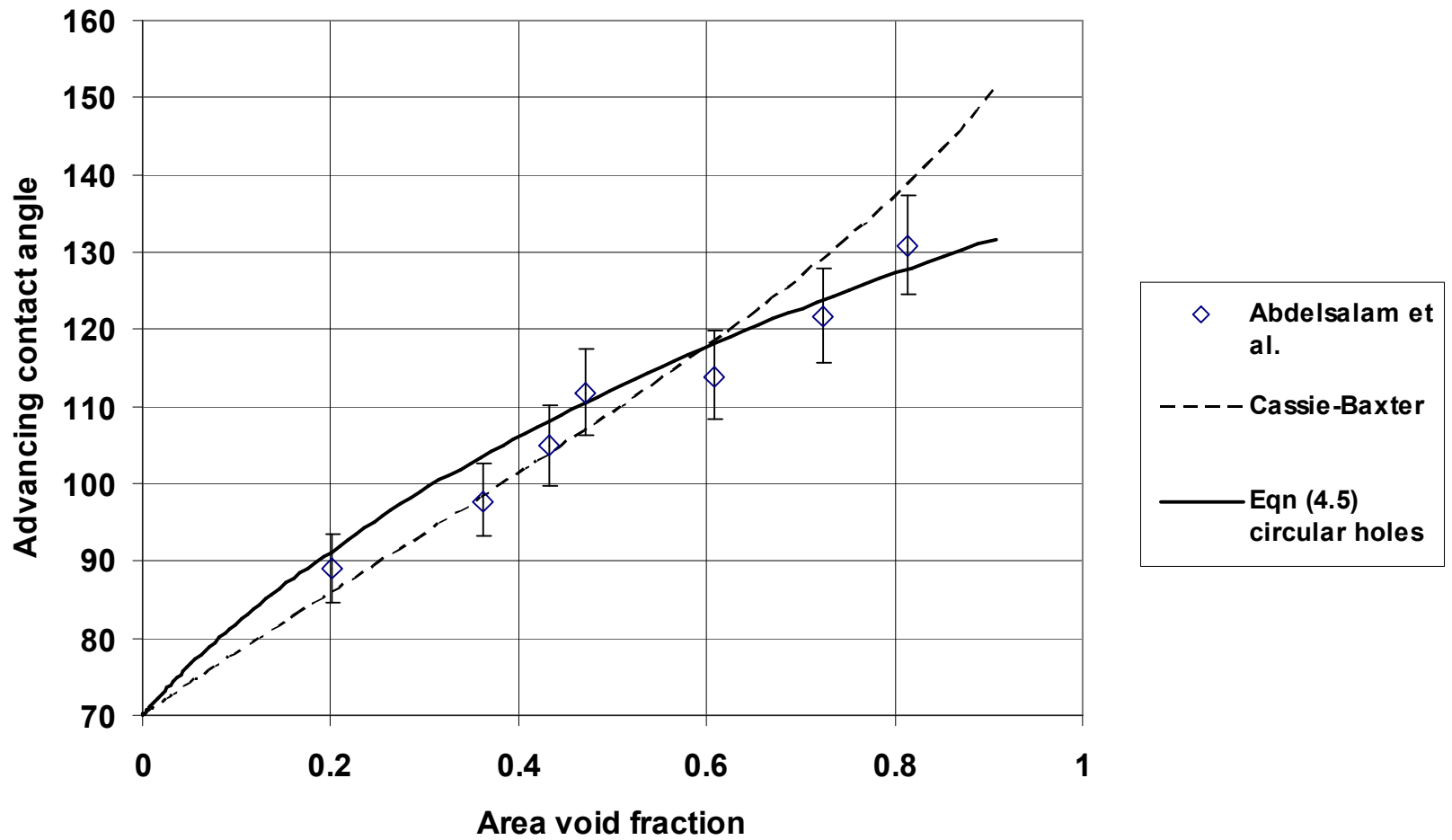


Figure 4.13 Comparison of data from Abdelsalam et al. against Cassie-Baxter theory and current theory.

CHAPTER 5

CONCLUSIONS AND RECOMMENDATIONS

5.1 Conclusions

In the present study, contact angles were measured on various microstructured specimens ranging in characteristic length scale as well as area void fraction. In particular, two types of surfaces bearing square cross section poles and square cross-section holes arranged on a square grid at centers were considered for two different etch depths. The two types of surfaces of a constant area void fraction differed mainly in the three-phase contact line topology of sessile drops placed on them. Conventional Cassie-Baxter theory [1] dictates that the area void fraction alone controls the resulting contact angle following Gibbs free energy minimization arguments on both types of surfaces.

The experimental measurements of advancing contact angles on the surfaces with the square poles were found to closely follow Cassie-Baxter theory. In contrast, the advancing contact angles on surfaces with square holes or continuous contact lines were observed to be independent of area void fraction. In addition the three-phase contact line topology was observed to significantly affect the dependence of the contact angle on the area void fraction. An optimum value of the characteristic length scale was identified for the maximum contact angle in the case of surfaces with square poles. An increase in the characteristic length scale resulted in wetting behavior proposed by the Wenzel theory. Further, an increase in the etch depth improved the hydrophobic behavior.

In the case of the homogenous wetting state, it was observed that air remains trapped especially for the surfaces with holes, thus not always achieving the Wenzel state. The contact angles for the specimen with holes, for this reason, were observed to be higher than those for the specimen with poles. However, the Wenzel state was achieved for the 3μ specimen and specimen with 0.75 area void fraction, in which case, the grooves were easily wetted due to the force with which the drop was placed on the surface.

On surfaces with discontinuous three-phase contact lines, the contact angle closely follows the prediction of the Cassie-Baxter theory which is in agreement with results reported in the literature. This trend is observed to be independent of the etch depth. However, for surfaces where sessile drops exhibit a continuous three-phase contact line, the advancing angle is observed to be independent of the area void fraction and the characteristic length scale and is governed by the total pinning force exerted by the surface defects. In cases where point defects dominate the contact line pinning behavior such as the surfaces considered in the present study, the advancing contact angles measured are independent of area void fraction, f , in accord with the number defect density on the contact line being independent of f . On the other hand, a chemically heterogeneous surface where the different regions of heterogeneity are separated by continuous and differentiable curves is expected to be dominated by edge defects rather than point defects. In such cases, the total contact line length pinned along the defect heterogeneity edge is a function of the area void fraction. Here we expect that the contact angle be a non-linear function of the area void fraction. For results on circular holes, we find that the pinned contact line dependence on the area void fraction fits the

experimental data to good accord. Therefore, the fundamental behavior of sessile drops on surfaces where the three-phase contact line is continuous is governed by defect pinning and not either by area or line fraction of the heterogeneities.

5.2 Recommendations

Contact line topology is very important to understanding the behavior of the liquid drop on surfaces and to achieve the surfaces of desired characteristics. Thus, an extensive study on the three-dimensional drop shapes, and further the dynamic behavior of the expanding and receding contact line on different topological surfaces through experimental and modeling techniques understanding the effect of this contact line on the apparent contact line will amount to a significant contribution to this area of research.

REFERENCES

1. Cassie, A.B.D. and S. Baxter, *Wettability of porous surfaces*. 1944: p. 546-551.
2. Wenzel, R.N., *Resistance of solid surfaces to wetting by water*. Industrial & Engineering Chemistry, 1936. **28**(8): p. 988-994.
3. Zhao, N., et al., *Fabrication of biomimetic superhydrophobic coating with a micro-nano binary structure*. Macromolecular rapid communications, 2005. **26**: p. 1075-1080.
4. Oner, D., and McCarthy, T.J., *Ultrasuperhydrophobic surfaces, effects of topography length scales on wettability*. Langmuir, 2000. **16**: p. 7777-7782.
5. Zhai, L., et al., *Patterned superhydrophobic surfaces: Toward a synthetic mimic of the Namib Desert beetle*. Nano Letters, 2006. **6**(6): p. 1213-1217.
6. Bartolo, D., et al., *Bouncing or sticky droplets: Impalement transitions on superhydrophobic micropatterned surfaces*. Europhysics Letters, 2006. **74**(2): p. 299-305.
7. Baldacchini, T., et al., *Superhydrophobic surfaces prepared by microstructuring of silicon using a femtosecond laser*. Langmuir, 2006. **22**(11): p. 4917-4919.
8. He, B., Lee, J. and Patankar, N.A., *Contact angle hysteresis on rough hydrophobic surfaces*. Colloid and Surfaces A, 2004. **248**: p. 101-104.
9. Iwamatsu, M., *Contact angle hysteresis of cylindrical drops on chemically heterogeneous striped surfaces*. Journal of Colloid and Interface Science, 2006. **297**(2): p. 772-777.
10. Chen, Y., He, B., Lee, J., and Patankar, N.A., *Anisotropy in the wetting of rough surfaces*. Journal of Colloid and Interface Science, 2005. **281**: p. 458-464.
11. He, B., N.A. Patankar, and J. Lee, *Multiple equilibrium droplet shapes and design criteria for rough hydrophobic surfaces*. Langmuir, 2003. **19**: p. 4999-5003.

12. McHale, G., et al., *Analysis of droplet evaporation on a superhydrophobic surface*. Langmuir, 2005. **21**(24): p. 11053-11060.
13. Gao, L., McCarthy, T.J., *The "Lotus effect" Explained: Two reasons why two length scales of topography are important*. Langmuir, 2006. **22**: p. 2966-2967.
14. Ramos, S. and A. Tanguy, *Pinning-depinning of the contact line on nanorough surfaces*. European Physical Journal E, 2006. **19**(4): p. 433-440.
15. Extrand, C.W., *Contact angles and hysteresis on surfaces with chemically heterogeneous islands*. Langmuir, 2003. **19**(9): p. 3793-3796.
16. Good, R.J., *Contact angle, wetting and adhesion: a critical review*. J. Adhesion Sci. Tech., 1992. **6**(12): p. 1269-1302.
17. H.Fleundlich, *Colloid and Capillary Chemistry*. Dutton. 1923, Newyork. 161.
18. Chaudhury, M.K., and Whitesides, G.M., *Correlation between surface energy and surface constitution*. Science, 1992. **255**: p. 1230-1232.
19. Timmons, C.O. and W.A. Zisman, J. Colloid Interface Sci., 1966. **22**: p. 165.
20. Chui, N.C. 1991, State University of Newyork at Buffalo.
21. Good, R.J. and M.L. Koo, J. Colloid Interface Sci., 1979. **71**.
22. Huang, H.T.L. 1990, State University of NewYork at Buffalo.
23. Enrique, R. *Measuring Dynamic Contact Angles by the Wilhelmy Plate method*. in *American Physical Society, Division of Fluid Dynamics Meeting*. 1997.
24. Madau, M.J., *Fundamentals of microfabrication*. 1997: CRC press.
25. Iwamatsu, M., *The validity of Cassie's law: A simple exercise using a simplified model*. Colloid and Interface Science, 2006. **294**: p. 176-181.

26. Cheng, Y.-T., Rodak, D.E., Wong, C.A. and Hayden, C.A., *Effects of micro- and nano-structures on the self-cleaning behaviour of lotus leaves*. Nanotechnology, 2006. **17**: p. 1359-1362.
27. Lacroix, L.M., et al., *Tuneable rough surfaces: A new approach for elaboration of superhydrophobic films*. Surface Science, 2005. **592**(1-3): p. 182-188.
28. Bhushan, B. and Y.C. Jung, *Micro- and nanoscale characterization of hydrophobic and hydrophilic leaf surfaces*. Nanotechnology, 2006. **17**(11): p. 2758-2772.
29. Feng, L., Li, S., Li, Y., Li, H., Zhang, L., Zhai, J., Song, Y., Liu, B., Jiang, L., Zhu, D., *Super-Hydrophobic Surfaces: From Natural to Artificial*. Advanced Materials, 2002. **14**(24): p. 1857-1860.
30. Hikita, M., et al., *Super-liquid-repellant surfaces prepared by colloidal silica nanoparticles covered with fluoroalkyl groups*. Langmuir, 2005. **21**: p. 7299-7302.
31. Shang, H.M., et al., *Optically transparent superhydrophobic silica-based films*. Thin Solid Films, 2005. **472**: p. 37-43.
32. Jia, X., and McCarthy, T.J., *Controlled Growth of Silicon Dioxide from nanoholes in silicon-supported tris-(trimethoxysiloxy)silyl monolayers: rational control of surface roughness at the nanometer length scale*. Langmuir, 2003. **19**: p. 2449-2457.
33. Liu, H., et al., *Reversible wettability of a chemical vapor deposition prepared ZnO film between superhydrophobicity and superhydrophilicity*. Langmuir, 2004. **20**: p. 5659-5661.
34. Qian, B., and Shen, Z., *Fabrication of Superhydrophobic Surfaces by Dislocation-Selective Chemical Etching on Aluminum, Copper and Zinc substrates*. Langmuir, 2005. **21**: p. 9007-9009.

35. Zorba, V., et al., *Making silicon hydrophobic: wettability control by two-lengthscale simultaneous patterning with femtosecond laser irradiation*. Nanotechnology, 2006. **17**(13): p. 3234-3238.
36. Patankar, N.A., *Mimicking the Lotus Effect: Influence of Double Roughness Structures and Slender Pillars*. Langmuir, 2004. **20**: p. 8209-8213.
37. Lafuma, A. and D. Quere, Nat. Mat., 2003. **2**(7): p. 457.
38. Bico, J., C. Marzolin, and D. Quere, *Pearl drops*. Europhys. Lett., 1999. **47**(2): p. 220-226.
39. Patankar, N.A., *On the modeling of hydrophobic contact angles on rough surfaces*. Langmuir, 2003. **19**: p. 1249-1253.
40. Dupuis, A., and Yeomans, J.M., *Modeling droplets on superhydrophobic surfaces: equilibrium states and transitions*. Langmuir, 2005. **21**: p. 2624-2629.
41. Patankar, N.A., *Transition between superhydrophobic states on rough surfaces*. Langmuir, 2004. **20**: p. 7097-7102.
42. Marmur, A., *Wetting on hydrophobic rough surfaces: to be heterogeneous or not to be?* Langmuir, 2003. **19**: p. 8343-8348.
43. Ishino, C., Okumura, K., and Quere, D., *Wetting transitions on rough surfaces*. Eur. Physical Journal E, 2004. **68**(3): p. 419-425.
44. Yang, J.T., et al., *Droplet manipulation on a hydrophobic textured surface with roughened patterns*. Journal of Microelectromechanical Systems, 2006. **15**(3): p. 697-707.
45. Bico, J., et al., *Wetting of textured surfaces*. Colloid and Surfaces A, 2002. **206**: p. 41-46.
46. Cheng, Y.-T., and Rodak, D.E., *Is the lotus leaf superhydrophobic?* Applied Physics Letters, 2005. **86**: p. 144101.

47. Extrand, C.W., *Designing for optimum liquid repellency*. Langmuir, 2006. **22**(4): p. 1711-1714.
48. Gao, L. and T.J. McCarthy, *How Wenzel and Cassie Were Wrong*. Langmuir, 2007. 23: p. 3762-3765.
49. Gao, L.a.M., T.J., *Contact Angle Hysteresis Explained*. Langmuir, 2006. 22: p. 6234-6237.
50. Cassie, A.B.D., *Contact angles. Discussions of the Faraday Society*, 1948. 3: p. 11-16.
51. Extrand, C.W., *Criteria for ultrahydrophobic surfaces*. Langmuir, 2004. 20: p. 5013-5018.
52. Extrand, C.W., *Model for contact angles and hysteresis on rough and ultraphobic surfaces*. Langmuir, 2002. 18(21): p. 7991-7999.
53. Abdelsalam, M.E., et al., *Wetting of regularly structured gold surfaces*. Langmuir, 2005. 21: p. 1753-1757.

VITA

Neeharika Anantharaju was born in Guntur, Andhra Pradesh, India, on March 17, 1983. Her elementary and high school education was in Guntur from Sri Venkateswara Bala Kuteer. In 2000, she entered Sri Chundi Ranganayakulu Engineering College, Guntur, affiliated with Jawaharlal Nehru Technological University, for her undergraduate studies and received the degree of Bachelor of Technology in Mechanical Engineering in June 2004. She entered Tennessee Technological University in August 2005 and is a candidate for the Master of Science degree in Mechanical Engineering.